R. & M. No. 3709

R. & M. No. 3709

MINISTRY OF DEFENCE (PROCUREMENT EXECUTIVE)

AERONAUTICAL RESEARCH COUNCIL
REPORTS AND MEMORANDA

Discrete Frequency Sound Generation in Axial Flow Turbomachines

By S. N. Smith
University Engineering Dept., Cambridge

LONDON: HER MAJESTY'S STATIONERY OFFICE
1973
PRICE £2·10 NET

Discrete Frequency Sound Generation in Axial Flow Turbomachines

By S. N. Smith
University Engineering Dept., Cambridge

Reports and Memoranda No. 3709*
March, 1972

Summary

A calculation method is described for unsteady, subsonic flow through an infinite, two-dimensional cascade of flat plate blades at zero mean incidence. The unsteady blade lift and moment, generated acoustic waves and shed vortex wakes can be calculated when the blades are subjected to bending or torsional vibration, incoming acoustic waves, or convected wake velocity perturbations. The results are in good agreement with those obtained by existing methods, and demands upon computer time and storage are slight.

Measurements have been made of the acoustic waves generated by a single compressor rotor excited by a convected wake velocity perturbation, with the blades in both an unloaded and a loaded condition. Agreement between theory and experiment is good in the unloaded blade case, but the present theory is inadequate to deal with the extra sound sources introduced by blade steady loading, and underestimates the generated wave amplitude in this case.

LIST OF CONTENTS

* Replaces A.R.C. 33 574.

LIST OF CONTENTS—*continued*

Section

1. Introduction

1.1. General

Throughout the early development of turbomachinery a designer's main preoccupation was the achievement of satisfactory aerodynamic performance. The sound generated by such machines represents a negligibly small energy loss, and if it was considered at all was regarded as a problem of relatively low importance. In more recent times the increasing size and range of application of turbomachines, particularly in the field of aerospace engineering, has led to a public exposure to noise which at least is unpleasant and at worst is actively harmful. Added to this are the dangers of acoustic fatigue of surrounding structures and damage to sensitive mechanisms nearby, with the result that noise reduction is now a leading priority in the further development of turbomachinery.

A wide variety of acoustical problems is involved, including the generation of noise by the exhaust jet of an aero-engine, the mechanisms of sound production in rotating and stationary blade rows, the transmission and reflection of sound in ducts containing more blade rows and other obstacles, and the radiation of sound into free space from duct openings. The sound generated by blade rows is found generally to consist of two components, a white noise background of relatively low amplitude and superimposed upon this a number of large amplitude tones at certain discrete frequencies. White noise has its origins in random turbulence in the airflow through the turbomachine, non-periodic force fluctuations on solid bodies in the flow—which may be caused by vortex shedding, boundary layer pressure fluctuations, blade vibration or incoming flow perturbations—and non-periodic interactions in the flow field between externally introduced perturbations and those associated with the blade row itself. However, it is now known that much of what was once considered to be broad band noise consists of discrete tones closely spaced in the frequency spectrum, and this together with the large amplitude of some of the tones means that they are the more immediate problem.

Discrete tones may be generated by one of a number of mechanisms, the nature of the sound source formed varying with the mechanism. Periodic displacement of fluid by the passage of blades generates sound which is monopole in character; fluctuating forces caused by vibration or regular flow disturbances are equivalent to dipole sound sources. Periodic interactions between perturbed quantities in the flow field, or between flow perturbations and blade thickness or loading, lead to the formation of a number of sources (Ref. (1)); in particular the interaction between fluctuating velocity components gives a quadrupole source field distributed throughout the flow (Ref. (2)). The distinction between broad-band noise and discrete tones is sometimes blurred, and large scale turbulence may give rise to peaks at discrete frequencies under suitable circumstances (Ref. (3)).

The present study is confined to the generation of discrete frequency sound by fluctuating blade forces, and the reflection and transmission of sound waves by blade rows employing a similar mechanism. The problems of blade vibration and vortex wake shedding are considered as an adjunct.

1.2. Previous Work

Much early work on the generation of noise in turbomachines was based upon attempts to obtain empirical relationships between the intensity of the sound produced and design parameters such as blade tip speed, and upon qualitative suggestions for noise reduction. Lowson[4] made a large number of such suggestions; Nemec[5,6] investigated the effect of blade bevelling; Moravec[7] suggested the introduction of secondary air at the blade trailing edges to reduce the wake momentum deficit; Smith and House[8] obtained empirical equations based on measurements made on a complete engine. A series of rather more sophisticated prediction methods took the values of fluctuating lift and moment calculated by Kemp and Sears[9,10] for potential flow and viscous wake interactions in incompressible flow, and by treating the lift force as a single dipole source, calculated the sound produced by such interactions. This approach was used by Hetherington,[11] Nemec, Lowson, and Bragg and Bridge,[12] who also made measurements on a single rotor compressor test rig. At about the same time Sharland[13] developed expressions for the prediction of broad-band noise generated by turbulence.

A different approach to the problem was typified by the work of Tyler and Sofrin,[14] who studied the permissible acoustic modes in annular and cylindrical ducts, and the conditions under which these

propagate or decay. They also demonstrated that interaction between blade rows could result in rotating pressure patterns that would couple into propagating duct modes, whereas an isolated subsonic rotor would excite only decaying modes. No attempt was made to predict the amplitude of the sound generated by a particular configuration, however, and the analysis assumes zero mean flow in the duct. The theory of Tyler and Sofrin was developed by Griffiths,[15] who also considered the effect of random modulation of the pure tone, and Morfey,[16] who included in his analysis the effects of waves reflected from the duct opening.

Later work has been primarily concerned with the solution of the equations of compressible flow through a blade row in order to calculate the amplitudes of sound waves generated, transmitted or reflected, the methods used differing widely in their choice of blade row models and mathematical techniques. Kaji and Okazaki[17] obtained a solution by representing each blade by an unsteady distribution of pressure doublets, and using the condition that there must be no net upwash at the blade surface to derive an integral equation for the unknown doublet distribution function, given a known input upwash perturbation. A simplified analysis based on semi-actuator disc theory, and giving good agreement with the more exact method for small blade spacing, was given by the same authors. A similar method to that used by Kaji and Okazaki was given by Carta,[18] who did not, however, attempt a complete solution but only considered the phenomenon of acoustic resonance or cut-off. Carta and Fanti[19] also gave a simplified physical explanation of this phenomenon, pointing out in particular that at resonance the aerodynamic damping and unsteady lift become zero. Mani[20] used the integral equation derived by Kaji and Okazaki, went some way towards a treatment of the kernel function singularities, and took as input perturbations the viscous wakes and potential flow field from an adjacent blade row.

Solutions to the reflection and transmission problems using the Wiener–Hopf technique were derived by Mani and Horvay[21] and Koch.[22] The first of these regarded the blades as semi-infinite in the direction of transmission in order to solve the reflection problem, and semi-infinite in the opposite direction to calculate the transmitted wave. Koch obtained rather more accurate results assuming finite blades and retaining some of the attenuated waveguide modes formed in the interblade space. The method of Mani and Horvay improves as the ratio of blade chord to acoustic wavelength is increased, but both methods are in good agreement with the results of Ref. (17). An alternative solution to the same problem, suitable when the ratio of blade chord to acoustic wavelength is small, was given by Amiet and Sears,[23] who used the method of matched asymptotic expansions. The blade force was calculated using quasi-steady Prandtl–Glauert theory and the result used in an acoustic dipole calculation. Again agreement with the results of Ref. (17) is good, except close to the cut-off condition for the blade row.

Whitehead[24] developed a calculation method applicable to the transmission and reflection problems, and to the generation of sound by vibration and incoming flow disturbances, based upon the work of Lane and Friedman.[25] This takes harmonic solutions to the reduced wave equation and superimposes these with respect to an unknown function of wavenumber to satisfy the conditions of zero upwash at the blade surfaces, and zero pressure jump off the blades. An integral equation for the unknown wavenumber function is set up, and the acoustic and aerodynamic properties of the blade row are given in terms of this function. The results agree closely with those of Refs. (17) and (25).

Approximate solutions to the generation problem using simplified blade row models were given by Mani,[26] and Benzakein and Kazin.[27,28] Mani represented the blades by a set of point forces, while Benzakein and Kazin used a rotating line vortex model. Measurements in support of Ref. (26) were carried out by Mani and Lipstein[29] on a single compressor rotor excited by the wakes from an array of cylindrical rods, and gave reasonable agreement with the theoretical predictions.

1.3. Present Work

The present study includes a theoretical and an experimental investigation into the problems of sound generation, transmission and reflection by a blade row. A calculation method is presented in Section 2 for an infinite two-dimensional cascade of flat plate blades operating at zero mean incidence, in which the cascade is replaced by a series of continuous singularity distributions. Solutions of the flow equations for each of these are summed together to give a solution for the complete cascade. The method is to some

extent similar to that of Ref. (17), in that basic solutions harmonic in the cascade direction are eventually summed together, but the approach used here leads to considerable mathematical simplification. Furthermore, the numerical method used in the solution of the integral equation for the unknown blade loading distribution, which includes a treatment of the kernel function singularities, gives a small and rapid computer program with the economic advantages which this entails.

In Section 3 details are given of experiments carried out on a single rotor compressor test rig, with the blade excitation provided by the wakes from a set of upstream gauzes. The blades were first run with zero steady loading, in order to check the prediction of the sound generated, given by the analysis of Section 2, then in a loaded condition to test the validity of the analysis when applied to this case. The results of this investigation are described in Section 4, and the conclusions of the study are summarised in Section 5.

2. Theoretical Analysis

2.1. Flow Model

The cascade flow model used in this analysis is shown in Fig. 1. The following assumptions are made:

(i) The system is two-dimensional. This means that bending vibration of a blade may be represented by translational motion of the equivalent two-dimensional aerofoil in a direction normal to the chord line, and that torsional blade vibration becomes simply rotation about a fixed axis.

(ii) The blades are flat plates of negligible thickness.

(iii) Effects of viscosity are neglected. There are therefore no boundary layers on the blades and the flow follows the blade surface without stalling.

(iv) The mean angle of incidence is zero. There is no steady blade loading and the mainstream flow passes through the cascade undeflected.

(v) All perturbations from the uniform mean flow are small, so that the flow equations may be linearised and the principle of superposition may be applied to the solutions obtained.

(vi) Events occurring at any particular blade are duplicated at all other blades, with a constant phase angle between each blade and its neighbour. This phase angle is an integral fraction of 2π.

(vii) The unsteady blade loading at the trailing edge is finite. This is the statement of the Kutta–Joukowski condition for unsteady flow.

(viii) The flow is subsonic.

(ix) The flow is isentropic.

2.2. Basic Equations

The linearised equations of momentum and continuity are

$$\frac{\partial \rho}{\partial t} + U\frac{\partial \rho}{\partial x} + V\frac{\partial \rho}{\partial y} + \rho_0\left(\frac{\partial u}{\partial x} + \frac{\partial v}{\partial y}\right) = 0,$$

$$\frac{\partial u}{\partial t} + U\frac{\partial u}{\partial x} + V\frac{\partial u}{\partial y} + \frac{1}{\rho_0}\frac{\partial p}{\partial x} = 0 \qquad (1)$$

and

$$\frac{\partial v}{\partial t} + U\frac{\partial v}{\partial x} + V\frac{\partial v}{\partial y} + \frac{1}{\rho_0}\frac{\partial p}{\partial y} = 0,$$

where U and V are the mean velocities in the x and y directions respectively; u and v are the corresponding unsteady velocity perturbations; ρ_0 and ρ are the mean and perturbation densities.

The flow is assumed to be isentropic, so that

$$\left(\frac{\partial p}{\partial \rho}\right)_s = \frac{dp}{d\rho} = a^2,$$

where a is the velocity of sound.

For harmonic space and time dependence the perturbation quantities may be written

$$\begin{vmatrix} u \\ v \\ p \end{vmatrix} = \begin{vmatrix} \bar{u} \\ \bar{v} \\ \bar{p} \end{vmatrix} \exp i(\omega t + \alpha x + \beta y), \tag{3}$$

in which $\bar{u}$, $\bar{v}$ and $\bar{p}$ are constant amplitudes and α and β are wave numbers. The vorticity in the flow is given by

$$\xi = \frac{\partial v}{\partial x} - \frac{\partial u}{\partial y} = \bar{\xi} \exp i(\omega t + \alpha x + \beta y),$$
$$\bar{\xi} = i\alpha\bar{v} - i\beta\bar{u}. \tag{4}$$

Using (2) and (3), equations (1) become

$$\begin{vmatrix} (\omega + U\alpha + V\beta) & a^2\alpha\rho_0 & a^2\beta\rho_0 \\ \alpha/\rho_0 & (\omega + U\alpha + V\beta) & 0 \\ \beta/\rho_0 & 0 & (\omega + U\alpha + V\beta) \end{vmatrix} \begin{vmatrix} \bar{p} \\ \bar{u} \\ \bar{v} \end{vmatrix} = 0, \tag{5}$$

and the condition for a non-trivial solution of (5) is

$$(\omega + U\alpha + V\beta)|(\omega + U\alpha + V\beta)^2 - a^2(\alpha^2 + \beta^2)| = 0. \tag{6}$$

Two different physical phenomena are embodied in (6) and these will be considered separately.

2.3. Pressure Waves

Equation (6) may be satisfied by setting

$$(\omega + U\alpha + V\beta)^2 - a^2(\alpha^2 + \beta^2) = 0. \tag{7}$$

Using this relationship in conjunction with (4) and (5) it follows that for perturbations of this type

$$\bar{\xi} = 0, \tag{8}$$

$$\frac{\bar{p}}{\bar{v}} = -\frac{(\omega + U\alpha + V\beta)\rho_0}{\beta} \tag{9}$$

and

$$\frac{\bar{u}}{\bar{v}} = \frac{\alpha}{\beta}. \tag{10}$$

This is therefore a case of irrotational pressure perturbations. Solving (7) for α in terms of β and ω, we have

$$\alpha = \frac{U(\omega + V\beta) \pm a\sqrt{(\omega + V\beta)^2 - (a^2 - U^2)\beta^2}}{a^2 - U^2}, \tag{11}$$

and with the assumption that β is real (which will be justified later) two possibilities arise depending upon the sign of the expression under the square root.

(a) $$(\omega + V\beta)^2 - (a^2 - U^2)\beta^2 > 0.$$

In this case α is real and disturbances propagate undiminished as acoustic waves.

(b) $$(\omega + V\beta)^2 - (a^2 + U^2)\beta^2 < 0.$$

Here α has an imaginary part, so that disturbances vary exponentially in amplitude with x. The sign outside the square root is chosen to satisfy the physical condition that these disturbances must decay as $|x| \to \infty$.

In both cases the two values of α correspond one to upstream going and the other to downstream going perturbations.

2.4. Vorticity Wave

Equation (6) may also be satisfied by writing

$$\omega + U\alpha + V\beta = 0. \tag{12}$$

It then follows from equations (5) that in this case

$$\bar{p} = 0, \tag{13}$$

$$\frac{\bar{u}}{\bar{v}} = -\frac{\beta}{\alpha} \tag{14}$$

and

$$\bar{\xi} = i\left(\alpha + \frac{\beta^2}{\alpha}\right)\bar{v}. \tag{15}$$

Solving (12) for α we have

$$\alpha = -\frac{(\omega + V\beta)}{U}, \tag{16}$$

so that for real β, α is always real and disturbances of this type propagate as vorticity waves with no associated pressure fluctuations. It is a simple matter to show that the phase velocity of the vorticity wave is equal to the component of the mainstream velocity in the direction normal to the wave front, and therefore that this wave is simply a spatial vorticity distribution being convected downstream by the mainstream flow.

2.5. Solution for a Vortex Row

The next step in the derivation of a solution for the complete cascade is to consider the effect of a row of bound vortices arranged along the y-axis as shown in Fig. 2. The vortices fluctuate in strength with amplitude Γ and angular frequency ω, with a constant phase angle ϕ between each vortex and its immediate neighbour. The strength of the mth vortex is therefore $\Gamma \exp i(\omega t + m\phi)$. It is shown in Appendix I that such a vortex row may be represented by a series of continuous wave-like sheets of vorticity moving in the y-direction, as follows:

$$\gamma(y) = \bar{\gamma}(y) \exp i\omega t = \sum_{r=-\infty}^{\infty} \frac{\Gamma}{s} \exp i\left\{\omega t + \frac{\phi - 2\pi r}{s} y\right\}, \tag{17}$$

where s is the vortex spacing and γ is the vortex strength per unit length along the y-axis. These sheets, all of which have the same amplitude Γ/s, will be called 'cascade-waves'.

In order for the flow perturbations produced by a single cascade-wave to be compatible with the wave itself they must have the same wave-number in the y-direction, that is,

$$\beta = \frac{\phi - 2\pi r}{s} \tag{18}$$

for pressure and vorticity fluctuations alike, where r is the index of the cascade-wave. This is the justification for the earlier assumption that β is real. The wavenumbers α may now be calculated in terms of ω, ϕ and the mainstream flow velocity from equations (11) and (16) for the different types of flow perturbation.

To calculate the magnitudes of the perturbations produced by the cascade-wave, the conditions to be satisfied by these perturbations must be examined. Upstream of the cascade wave only the upstream going pressure perturbation can exist, while downstream both the downstream going pressure perturbation

and the convected vorticity wave may be present. Quantities associated with these different phenomena will be distinguished by suffices as follows:

Upstream pressure perturbation—suffix 1

Downstream pressure perturbation—suffix 2

Convected vorticity wave—suffix 3.

The equation of continuity through the cascade-wave is then

$$(U + u_1)(\rho_0 + \rho_1) = (U + u_2 + u_3)(\rho_0 + \rho_2)$$

since $\rho_3 = 0$. Expanding, neglecting terms of second order in fluctuating quantities, and dividing throughout by $\exp i(\omega t + \beta y)$ we have

$$U\bar{\rho}_1 + \bar{u}_1\rho_0 = U\bar{\rho}_2 + \bar{u}_2\rho_0 + \bar{u}_3\rho_0.$$

Re-writing in terms of $\bar{v}_1, \bar{v}_2$ and $\bar{v}_3$ using equations (2), (9), (10) and (14),

$$\left\{\alpha_1 - \frac{U}{a^2}(\omega + U\alpha_1 + V\beta)\right\}\bar{v}_1 = \left\{\alpha_2 - \frac{U}{a^2}(\omega + U\alpha_2 + V\beta)\right\}\bar{v}_2 - \frac{\beta^2}{\alpha_3}\bar{v}_3. \tag{19}$$

Secondly, the velocity jump in the y-direction as the cascade-wave is crossed must be equal to the strength of the wave itself, so that

$$\bar{v}_2 + \bar{v}_3 - \bar{v}_1 = \Gamma/s. \tag{20}$$

Finally, since the convected vorticity wave consists of vorticity which is continuously shed from the cascade-wave, the strengths of the two must be related. It is shown in Appendix II that this relationship is given by

$$\bar{\xi} = -i\frac{\omega\Gamma}{Us}. \tag{21}$$

Using equation (15) this becomes

$$\left(\alpha_3 + \frac{\beta^2}{\alpha_3}\right)\bar{v}_3 = -\frac{\omega\Gamma}{Us}. \tag{22}$$

Equations (19), (20) and (22) may now be solved for the three unknown velocity perturbations $\bar{v}_1$, $\bar{v}_2$ and $\bar{v}_3$, giving:

$$\bar{v}_{1,2} = \frac{\Gamma}{s}\frac{\hat{\beta}^2}{2A}\left(\mp 1 \mp \frac{\lambda}{\beta}\sin\theta + \frac{i\lambda\cos\theta}{\sqrt{\hat{\beta}^2 - M^2A}}\right) \tag{23}$$

and

$$\bar{v}_3 = \frac{\Gamma}{s}\frac{\lambda^2 + \hat{\beta}\lambda\sin\theta}{A}, \tag{24}$$

where the upper sign in (23) refers to $\bar{v}_1$, the lower to $\bar{v}_2$, and

$$\lambda = \frac{\omega c}{W},$$

$$W = \sqrt{U^2 + V^2}$$

and

$$\hat{\beta} = \beta c,$$

c = a normalising length which later will coincide with the blade chord length,

$$\theta = \tan^{-1}\frac{V}{U},$$

$$M = \frac{W}{a}$$

and

$$A = \lambda^2 + \hat{\beta}^2 + 2\lambda\hat{\beta}\sin\theta.$$

The fluctuating quantities $\bar{p}$ and $\bar{u}$ are calculated from the values for $\bar{v}$ using equations (9), (10) and (14). The total effect of the complete vortex row is now obtained by simply summing together the effects of all the constituent cascade waves:

$$v_{1,2,3}(\text{total}) = \sum_{r=-\infty}^{\infty} \bar{v}_{1,2,3} \exp i(\omega t + \alpha_{1,2,3} x + \beta y) \tag{25}$$

where

$$\left(\beta = \frac{\phi - 2\pi r}{s}\right).$$

Here any single value of the multiple suffix may be taken throughout.

These expressions are equivalent to those derived by Kaji[17] for the doublet row.

2.6 Derivation of Upwash Integral Equation for Cascade

Each chordal element dz of the cascade shown in Fig. 1 forms a vortex row, and may be described as a series of cascade waves of the form

$$\bar{y}(y) = \sum_{r=-\infty}^{\infty} \frac{\Gamma(z_0)\, dz_0}{s} \exp i\left\{\frac{(\phi - 2\pi r)}{s}(y - y_0)\right\} \tag{26}$$

for the element at z_0. Here $\Gamma(z)$ is the blade vorticity distribution, ϕ the interblade phase angle, and z is a co-ordinate measured from the blade leading edge in the chordal direction. The induced upwash velocities normal to the chord at the point z on the reference blade are of the form

$$\frac{\Gamma(z_0)\, dz_0}{s} \sum_{r=-\infty}^{\infty} (v' \cos\theta - u' \sin\theta) \exp i\{\omega t + (\alpha \cos\theta + \beta \sin\theta)(z - z_0)\} \tag{27}$$

where u', v' are defined by

$$\left|\begin{matrix} u' \\ v' \end{matrix}\right| \frac{\Gamma}{s} = \left|\begin{matrix} \bar{u} \\ \bar{v} \end{matrix}\right| \tag{28}$$

and $\bar{u}, \bar{v}$ are given by equations (23), (24), (10) and (14). If $(z - z_0) < 0$, the relevant velocities are those associated with the upstream pressure perturbation; if $(z - z_0) > 0$, those associated with the downstream pressure perturbation and convected vorticity wave must be taken. The total upwash $w(z) \exp(i\omega t)$ induced by the whole cascade is evaluated by integration along the blade chord. Thus

$$\begin{aligned} w(z) = \int_0^z \frac{\Gamma(z_0)}{s} \sum_{r=-\infty}^{\infty} & |(v_2' \cos\theta - u_2' \sin\theta) \exp i\{(\alpha_2 \cos\theta + \beta \sin\theta)(z - z_0)\} \\ & + (v_3' \cos\theta - u_3' \sin\theta) \exp i\{(\alpha_3 \cos\theta + \beta \sin\theta)(z - z_0)\}|\, dz_0 \\ & + \int_z^c \frac{\Gamma(z_0)}{s} \sum_{r=-\infty}^{\infty} (v_1' \cos\theta - u_1' \sin\theta) \exp i\{(\alpha_1 \cos\theta + \beta \sin\theta)(z - z_0)\}\, dz_0, \end{aligned} \tag{29}$$

which is written as

$$\frac{w(\hat{z})}{W} = \int_0^1 \Gamma_w(\hat{z}_0) K(\hat{z} - \hat{z}_0)\, d\hat{z}_0, \tag{30}$$

where

$$K(\eta) = \frac{1}{(s/c)} \sum_{r=-\infty}^{\infty} |(v'_2 \cos\theta - u'_2 \sin\theta) \exp i(\hat{\alpha}_2 \cos\theta + \hat{\beta} \sin\theta)(\eta)$$

$$+ (v'_3 \cos\theta - u'_3 \sin\theta) \exp i(\hat{\alpha}_3 \cos\theta + \hat{\beta} \sin\theta)(\eta)| \quad \text{for } \eta > 0 \tag{31}$$

and

$$K(\eta) = \frac{1}{(s/c)} \sum_{r=-\infty}^{\infty} (v'_1 \cos\theta - u'_1 \sin\theta) \exp i(\hat{\alpha}_1 \cos\theta + \hat{\beta} \sin\theta)(\eta) \quad \text{for } \eta < 0,$$

$$\left| \begin{array}{l} \hat{\alpha} = \alpha c \\ \hat{z} = z/c \\ \Gamma_W = \Gamma/W \end{array} \right|.$$

Equation (30) is the upwash integral equation for the unknown vorticity distribution Γ_W, and may be solved with a given input velocity perturbation $(-w(\hat{z}))$ to satisfy the condition that there should be no net upwash at the blade surface.

2.7. Input Upwash Velocities

The five types of input perturbation used are the same as those considered by Whitehead.[24] They are briefly described here.

(i) Bending vibration of the blade with velocity normal to the chord-line $w_b \exp(i\omega t)$ gives

$$w(\hat{z}) = w_b. \tag{32}$$

(ii) Torsional vibration about the leading edge with angular displacement $\delta \exp(i\omega t)$ gives

$$w(\hat{z}) = W\delta(1 + i\lambda\hat{z}). \tag{33}$$

(iii) A convected sinusoidal wake perturbation inducing an upwash velocity $w_W \exp(i\omega t)$ at the leading edge of the reference blade gives

$$w(\hat{z}) = -w_W \exp(-i\lambda\hat{z}). \tag{34}$$

(iv) An upstream going acoustic wave incident upon the cascade from downstream gives an upwash velocity of the form

$$w(\hat{z}) = -w_u \exp\{i(\hat{\alpha}_u \cos\theta + \hat{\beta}_u \sin\theta)\hat{z}\}. \tag{35}$$

(v) Similarly, for a downstream going acoustic wave

$$w(\hat{z}) = -w_d \exp\{i(\hat{\alpha}_d \cos\theta + \hat{\beta}_d \sin\theta)\hat{z}\}. \tag{36}$$

In cases (iv) and (v) the wavenumbers α and β must satisfy equation (11).

2.8. Far Field Acoustic Waves

A particular cascade wave excites acoustic perturbations in the flow which may propagate unattenuated or decay exponentially away from the cascade, depending on its value of β and therefore of r, $\{\beta = (\phi - 2\pi r)/s\}$. Which alternative will apply in a given case is determined by the condition set out in Section 2.3. If decaying perturbations are produced the mode is said to be 'cut-off'. For a particular set of cascade parameters there is a definite value of $|r|$ above which all modes are cut off, exciting perturbations with increasing decay rates as $|r|$ increases. As M approaches unity this limiting value of $|r|$ becomes infinite. For each value of r which gives a propagating mode, a pair of waves is formed, one travelling upstream and the other downstream. The waves produced in such a mode by the chordal element dz_0 at z_0 are of the form

$$p_{1,2} = \frac{1}{s}\Gamma(z_0)p'_{1,2} \exp(i\omega t + i\alpha_{1,2}(x - x_0) + i\beta(y - y_0))\, dz_0 \tag{37}$$

where the suffices have the same meanings as before. From equation (9)

$$\frac{p'_{1,2}}{v'_{1,2}} = -\frac{(\omega + U\alpha_{1,2} + V\beta)\rho_0}{\beta} \tag{38}$$

and $v'_{1,2}$ is given by equations (23) and (28). Combining these and integrating over the chord gives the total amplitudes of the waves in this mode:

$$\frac{\bar{p}_{1,2}}{\rho_0 W^2} = -\frac{1}{(s/c)} v'_{1,2} \frac{(\lambda + \hat{\alpha}_{1,2}\cos\theta + \hat{\beta}\sin\theta)}{\hat{\beta}} \int_0^1 \Gamma_W(\hat{z}_0) \exp\{-(i\hat{\alpha}_{1,2}\cos\theta + \hat{\beta}\sin\theta)\hat{z}_0\}\, d\hat{z}_0 \tag{39}$$

2.9. Lift and Moment

Whitehead[30] has shown that the lift force acting on a blade is given by

$$F = -\rho_0 W \int_0^c \Gamma(z_0)\, dz_0$$

which may be re-written as

$$C_L = \frac{F}{\rho_0 W^2 c} = -\int_0^1 \Gamma_W(\hat{z}_0)\, d\hat{z}_0. \tag{40}$$

Although this expression is derived in Ref. (30) for the incompressible case no alteration is necessary for application here. Similarly the moment acting about the leading edge is

$$M = -\rho_0 W \int_0^c z_0 \Gamma(z_0)\, dz_0$$

so that

$$C_M = \frac{M}{\rho_0 W^2 c^2} = -\int_0^1 \hat{z}_0 \Gamma_W(\hat{z}_0)\, d\hat{z}_0. \tag{41}$$

2.10. Shed Vortex Sheet

The vortex $\Gamma(z_0)\exp(i\omega t)\, dz_0$ sheds, in a time interval δt at $t = t_0$, a free vortex of strength $-i\omega\Gamma(z_0)\exp(i\omega t_0)\, dz_0\, \delta t$. The sheet of which this vortex forms a part, and which is convected at mainstream velocity W, is therefore of strength

$$\zeta = -\frac{i\omega\Gamma(z_0)\exp(i\omega t_0)\, dz_0\, \delta t}{W\, \delta t}.$$

Writing

$$t_0 = t - \frac{(z - z_0)}{W}$$

gives

$$\zeta = -\frac{i\omega\Gamma(z_0)\exp(i\omega z_0/W)\, dz_0}{W} \exp\left(i\omega t - \frac{i\omega z}{W}\right)$$

and integrating over the chord, the total amplitude of the sheet is given by

$$\frac{\bar{\zeta}}{W} = -i\lambda \int_0^1 \Gamma_W(\hat{z}_0)\exp(i\lambda\hat{z}_0)\, d\hat{z}_0. \tag{42}$$

2.11. Solution of the Upwash Integral Equation

The kernel function $K(\hat{z} - \hat{z}_0)$ of equation (30) contains two different types of infinite series, one corresponding to the convected vorticity wave and the other to the irrotational pressure perturbation. The vorticity wave series may be summed analytically, and it is shown in Appendix III that the result of this summation is given by

$$\sum_{r=-\infty}^{\infty} (v'_3 \cos\theta - u'_3 \sin\theta) \exp\{(i\hat{\alpha}_3 \cos\theta + i\hat{\beta}\sin\theta)(\eta)\}$$

$$= \frac{\lambda}{4}\frac{s}{c} \frac{\sinh(\lambda s/c \cos\theta)}{\sin^2\left(\frac{\phi}{2} + \frac{\lambda}{2}\frac{s}{c}\sin\theta\right) + \sinh^2\left(\frac{\lambda}{2}\frac{s}{c}\cos\theta\right)} \exp(-i\lambda\eta). \tag{43}$$

The remaining series are summed numerically, their convergence being assured by the exponential behaviour of the higher order terms.

The numerical method used in the solution of the integral equation follows closely that given by Whitehead[30] for the incompressible case. The following co-ordinate transformation is made:

$$\hat{z}_0 = \tfrac{1}{2}(1 - \cos\psi)$$

and

$$\hat{z} = \tfrac{1}{2}(1 - \cos\varepsilon) \tag{44}$$

and substitution in equation (30) gives

$$\int_0^{\pi} \Gamma_W K(\tfrac{1}{2}\cos\psi - \tfrac{1}{2}\cos\varepsilon)\tfrac{1}{2}\sin\psi \, d\psi = \frac{w(\frac{1}{2}(1 - \cos\varepsilon))}{W}. \tag{45}$$

The function Γ_W will be specified by its values at n points, given by

$$\psi = \frac{\pi l}{n} \qquad (l = 0, 1, \ldots, (n-1)).$$

The value of Γ_W at the trailing edge, when $l = n$, is indeterminate, since it is always multiplied by $\sin\psi$ which is zero at this point. Equation (45) may therefore be satisfied at n points, and these will be defined by

$$\varepsilon = \frac{\pi(2m+1)}{2n} \qquad (m = 0, 1, \ldots, (n-1)).$$

These values of ε lie midway between the values of ψ at which Γ_W is specified.

A difficulty arises in the numerical evaluation of the integral in equation (45), owing to the singular behaviour of the kernel function $K(\eta)$ when $\eta = 0$. The singularities are of two types, one behaving like $\{\sqrt{1 - M^2}\exp(iM^2\lambda\eta/1 - M^2)\}/2\pi\eta$ and the other like $f(\eta)\log|\eta|$ when η is small, where $f(\eta)$ is a well behaved function. The extraction of these singularities and the determination of $f(\eta)$ are carried out in Appendix IV. Whitehead[30] has shown that except for the logarithmic term the integration may be performed using the trapezoidal rule, while the logarithmic term itself may be treated by means of the following formula:

$$\int_0^{\pi} g(\psi)\log\tfrac{1}{2}|\cos\psi - \cos\varepsilon| \, d\psi = -\frac{2\pi}{n}\sum_{l=0}^{n}{}' g\left(\frac{\pi l}{n}\right)\left\{\log_e 2 + \sum_{r=1}^{n}{}' \frac{1}{r}\cos r\varepsilon \cos\frac{\pi r l}{n}\right\}, \tag{46}$$

where $\sum_{l=0}^{\prime n}$ denotes a summation in which the first and last terms are given half weight, and $\sum_{r=1}^{\prime n}$ a summation in which the last term only has half weight. Writing the kernel function as

$$K(\eta) = K'(\eta) + f(\eta)\log|\eta| \tag{47}$$

and carrying out the whole integration in this way, we have

$$\sum_{l=0}^{n}{}'\left[K'\left(\frac{1}{2}\cos\frac{\pi l}{n}-\frac{1}{2}\cos\frac{\pi\overline{2m+1}}{2n}\right)-2f\left(\frac{1}{2}\cos\frac{\pi l}{n}-\frac{1}{2}\cos\frac{\pi\overline{2m+1}}{2n}\right)\right.$$
$$\left.\times\left\{\log_e 2+\sum_{r=1}^{n}{}'\frac{1}{r}\cos\frac{\pi r(2m+1)}{2n}\cos\frac{\pi rl}{n}\right\}\right]\times\left[\frac{\pi}{2n}\sin\frac{\pi l}{n}\Gamma_W\right]$$
$$=\frac{w[\frac{1}{2}\{1-\cos(\pi\overline{2m+1})/2n\}]}{W}. \tag{48}$$

In this equation Γ_W symbolises five sets of unknown values, corresponding to the five different input upwash velocities. Distinguishing between these by writing

$$\Gamma_W=\left|\frac{w_b}{W}\Gamma_{Wb},\delta\Gamma_{W\delta},\frac{w_W}{W}\Gamma_{WW},\frac{w_u}{W}\Gamma_{Wu},\frac{w_d}{W}\Gamma_{Wd}\right|, \tag{49}$$

the equation may be written in matrix form as

$$\underline{K}\underline{\Gamma}=\underline{U} \tag{50}$$

where $\underline{K}$ is an $n\times n$ matrix with the element in the mth row and lth column given by the first term in square brackets in equation (48); $\underline{\Gamma}$ is an $n\times 5$ matrix with the lth row given by

$$|\Gamma_{Wb},\Gamma_{W\delta},\Gamma_{WW},\Gamma_{Wu},\Gamma_{Wd}|\frac{\pi}{2n}\sin\frac{\pi l}{n}$$

and $\underline{U}$ is an $n\times 5$ matrix whose mth row is

$$|1,1+i\lambda\hat{z},-\exp(-i\lambda\hat{z}),-\exp\{i(\hat{\alpha}_u\cos\theta+\hat{\beta}_u\sin\theta)\hat{z}\},-\exp\{i(\hat{\alpha}_d\cos\theta+\hat{\beta}_d\sin\theta)\hat{z}\}|$$

where

$$\hat{z}=\frac{1}{2}\left(1-\cos\frac{\pi\overline{2m+1}}{2n}\right).$$

The solution of equation (50) is then

$$\underline{\Gamma}=\underline{K}^{-1}\underline{U} \tag{51}$$

2.12. Numerical Evaluation of Acoustic Wave Amplitudes, Lift and Moment Coefficients, and Shed Wakes

Equation (39) for the acoustic wave amplitudes may be written

$$\frac{\bar{P}_{1,2}}{\rho_0 W^2}=\int_0^1 V_{1,2}(\hat{z}_0)\Gamma_W(\hat{z}_0)\,d\hat{z}_0 \tag{52}$$

where

$$V_{1,2}(\hat{z}_0)=-\frac{1}{(s/c)}v'_{1,2}\frac{(\lambda+\hat{\alpha}_{1,2}\cos\theta+\hat{\beta}\sin\theta)}{\hat{\beta}}\exp\{-(i\hat{\alpha}_{1,2}\cos\theta+\hat{\beta}\sin\theta)\hat{z}_0\}. \tag{53}$$

Integrating by the trapezoidal rule, as in the previous section, we have

$$\frac{\bar{P}_{1,2}}{\rho_0 W^2}=\sum_{l=0}^{n}{}'V_{1,2}\left(\frac{1}{2}\left(1-\cos\frac{\pi l}{n}\right)\right)\Gamma_W\frac{1}{2}\sin\frac{\pi l}{n}\frac{\pi}{n}, \tag{54}$$

The five different input perturbations are accommodated by means of a device similar to that used for Γ_W, a set of pressure coefficients being defined as follows:

$$\frac{\bar{P}_{1,2}}{\rho_0 W^2}=\left|\frac{w_b}{W}P_{1,2b},\delta P_{1,2\delta},\frac{w_W}{W}P_{1,2W},\frac{w_u}{W}P_{1,2u},\frac{w_d}{W}P_{1,2d}\right|. \tag{55}$$

An identical method is used for the lift and moment coefficients and the shed wakes. Equation (40) for the lift gives

$$\frac{F}{\rho_0 W^2 c} = -\sum_{l=0}^{n}{}' \Gamma_W \frac{1}{2} \sin\frac{\pi l}{n}\frac{\pi}{n}, \tag{56}$$

with a set of lift coefficients defined by

$$\frac{F}{\rho_0 W^2 c} = \left|\frac{w_b}{W}C_{Lb}, \delta C_{L\delta}, \frac{w_W}{W}C_{LW}, \frac{w_u}{W}C_{Lu}, \frac{w_d}{W}C_{Ld}\right|. \tag{57}$$

From equation (41) for the moment

$$\frac{M}{\rho_0 W^2 c^2} = -\sum_{l=0}^{n}{}' \Gamma_W \frac{1}{2}\left(1 - \cos\frac{\pi l}{n}\right)\frac{1}{2}\sin\frac{\pi l}{n}\frac{\pi}{n} \tag{58}$$

and

$$\frac{M}{\rho_0 W^2 c^2} = \left|\frac{w_b}{W}C_{Mb}, \delta C_{M\delta}, \frac{w_W}{W}C_{MW}, \frac{w_u}{W}C_{Mu}, \frac{w_d}{W}C_{Md}\right| \tag{59}$$

and from equation (42) for the shed vortex sheet

$$\frac{\bar{\zeta}}{W} = -i\lambda \sum_{l=0}^{n}{}' \Gamma_W \exp\left|\frac{i\lambda}{2}\left(1 - \cos\frac{\pi l}{n}\right)\right| \frac{1}{2}\sin\frac{\pi l}{n}\frac{\pi}{n} \tag{60}$$

and

$$\frac{\bar{\zeta}}{W} = \left|\frac{w_b}{W}\zeta_b, \delta\zeta_\delta, \frac{w_W}{W}\zeta_W, \frac{w_u}{W}\zeta_u, \frac{w_d}{W}\zeta_d\right|. \tag{61}$$

Equations (54), (56), (58) and (60) may be collected together and written in matrix form as

$$\underline{C} = \underline{X}\underline{\Gamma} \tag{62}$$

where

$$\underline{C} = \begin{vmatrix} P_{1b} & P_{1\delta} & P_{1W} & P_{1u} & P_{1d} \\ P_{2b} & P_{2\delta} & P_{2W} & . & . \\ C_{Lb} & C_{L\delta} & . & . & . \\ C_{Mb} & . & . & . & . \\ \zeta_b & . & . & . & . \end{vmatrix}.$$

$\underline{X}$ is a $5 \times n$ matrix whose lth column is

$$\begin{vmatrix} V_1\left(\frac{1}{2}\left(1 - \cos\frac{\pi l}{n}\right)\right) \\ V_2\left(\frac{1}{2}\left(1 - \cos\frac{\pi l}{n}\right)\right) \\ -1 \\ -\frac{1}{2}\left(1 - \cos\frac{\pi l}{n}\right) \\ -i\lambda \exp\left|\frac{i\lambda}{2}\left(1 - \cos\frac{\pi l}{n}\right)\right| \end{vmatrix}.$$

Substituting for Γ from equation (51) gives

$$\underline{C} = \underline{X}\underline{K}^{-1}\underline{U}. \tag{63}$$

The required output matrix $\underline{C}$ may be calculated from this expression, since the matrices $\underline{X}$, $\underline{K}$ and $\underline{U}$ are all known.

3. Experiments

3.1. Introduction

The experiments described in this Section were devised with the following objectives in mind:

(i) To test predictions of the sound generated by a blade row given by the analysis of Section 2.

(ii) To determine the extent to which these predictions are valid when the blades are at incidence, and consequently have finite steady loading.

Certain features of a suitable test rig were therefore already established:

(i) The blade loading had to be variable over a wide range, down to and including the unloaded condition, and the blades had to be capable of efficient operation over this range.

(ii) The flow had to be closely two-dimensional.

(iii) A means of introducing a suitable perturbation into the flow had to be included, in order to excite the acoustic response.

The chosen compromise consists of a low camber, high hub/tip ratio compressor-rotor running in a parallel walled annular duct. Sound waves in such a duct propagate in spiralling paths, but if radial effects are sufficiently small they may be regarded as two-dimensional. (This point is discussed further in Section 4.) Independently variable air inlet velocity and rotor speed enable the blade loading to be varied. A flow perturbation of the convected wake type is used, as this may easily be introduced by means of upstream obstacles, and in addition represents an important source of sound in practical turbomachines.

The details of this arrangement are described in the following sections.

3.2. Description of Apparatus—Air Supply

Apart from the test section itself the whole of the apparatus is concerned with the delivery of a variable flow-rate, quiet air supply to the rotor annulus. The overall layout is shown in Fig. 3.

Air enters the system through a Burgess 14 H silencer, which offers negligible resistance at the flow rates used in the experiments and which gives a sound attenuation of 50–55 dB in the frequency range of interest. The silencer discharges into a 849·5 litre (30 cu ft) settling chamber lined, as are the other settling chambers in the system, with Perfonit Satellite 21 1·9 cm ($\frac{3}{4}$ inch) wood-fibre acoustic tiling.

Following the settling chamber is a 38 cm (15 inch) Blackman centrifugal fan, with backward curved blades, which is capable of delivering 85 m^3/min (3000 cu ft/min) of air against a head of 15·2 cm (6 inches) of water. This is driven by a 5·6 kW (7·5 hp) electric motor coupled with a Wallwork variable speed drive unit, giving continuously controllable fan speed over a range of 5:1. A diffuser of area ratio 4:1 links the fan to a second settling chamber of the same type as before, reducing the air velocity to 3 m/sec (10 ft/sec) at a flow rate of 85 m^3/min (3000 cu ft/min) before entry to the chamber. The diffuser contains three horizontal and three vertical splitters. The flow at outlet from the fan is poorly distributed and a honeycomb is situated in the diffuser inlet in order to achieve acceptable uniformity.

Leaving the settling chamber the flow enters a Burgess 16 L silencer, again of negligible resistance at the flow rates used. The background noise level at outlet from this silencer was measured using a 1·27 cm. ($\frac{1}{2}$ inch) Bruel and Kjoer condenser microphone fitted with a nose cone, mounted in the outlet plane and coupled to a Bruel and Kjoer 2203 sound level meter and 1613 octave filter set. Octave spectra are shown in Fig. 4. The frequency range of particular interest in the experiments was 400–800 Hz, and it will be noted that the system does not achieve its best attenuation until frequencies higher than 1000 Hz are used. Experiments planned in a higher frequency range or the use of silencers more effective at low frequencies therefore suggest themselves as possible modifications in future work of this type.

A third and final settling chamber follows the silencer, and from here the flow enters a smooth contraction which leads to the test section. The contraction contains a nose cone which together with the contraction itself ultimately forms an annulus of the same dimensions as the rotor duct. The nose cone is supported by two cross pieces bolted to the settling chamber wall, so that disturbances introduced into the flow are smoothed by the subsequent acceleration. The total area ratio of contraction and nose cone is 5·6:1.

The entire apparatus is contained in a room whose walls and ceiling are lined with Treetex Slotac 1.9 cm ($\frac{3}{4}$ inch) wood-fibre acoustic panelling, mounted on wooden battens.

3.3. Description of Apparatus—Test Section

3.3.1. *Blade-wake geometry.* It is shown in Section 2 that when a blade row operates in a suitably perturbed flow a number of propagating acoustic wave pairs may be formed, depending upon the inter-blade phase angle and frequency of the disturbance, and the blade-relative Mach number of the flow. The object of the blade-wake structure used in this apparatus is to ensure that only one such wave pair is formed, all other modes being cut-off. Measurements are thereby simplified considerably.

To begin with, the perturbation introduced into the flow takes the form of a velocity fluctuation sinusoidal in the circumferential direction, superimposed on the main-stream velocity, so that in a rotor-fixed reference frame each blade encounters a disturbance at wake passing frequency only, with no higher harmonics. Secondly, there are 24 complete periods of this fluctuation in one circuit of the annulus, and 23 rotor blades, giving an interblade phase angle of $-2\pi/23$ radians. If flow conditions are taken to be representative at blade mid-span, and if the main-stream flow is axial in a stationary reference frame, then the frequency parameter in a blade fixed frame is given by

$$\lambda = \frac{\omega c}{W} = \frac{N_W c \sin\theta}{R_0} \tag{64}$$

where N_W = number of wakes, R_0 = duct radius at the blade mid-height, and the remaining symbols have their former meanings. In the experiments $c/R_0 = 0{\cdot}286$, θ is always between 26 and 33 degrees and the maximum blade-relative Mach number achievable is 0·13. Applying these figures to the cut-off condition of Section 2.3, it is easily shown that only the $r = 0$ mode can possibly propagate under these circumstances. Furthermore, calculation of the exponential decay term contained in the x-direction wavenumber of equation (11) for the next mode in the series, ($r = -1$), gives the decay rate of perturbations in this mode. At a blade-relative mach number of 0·13 this is approximately 50 dB per chordal distance measured axially away from the blade row. Perturbations in other modes decay at even higher rates, so that all modes except that for which $r = 0$ may be neglected. In a stationary reference frame the observed effect is then that of a single propagating wave at blade passing frequency.

Another way of looking at this situation is in terms of the interaction pattern model used by Tyler and Sofrin.[14] The 23 blade–24 sinusoidal wake configuration gives rise to a one-lobed interaction pattern rotating at 23 times rotor speed, and a series of multi-lobed patterns rotating at speeds such that the observed frequency in a stationary reference frame is blade passing frequency. Only the one-lobed pattern rotates at a speed high enough for propagation to occur, which leads to the same result as before.

3.3.2. *Test section—construction.* The construction of the test section is illustrated in Fig. 5. Many of the details are given in the figure and will not be described here.

To obviate the need for support struts, with their disturbing effect upon the flow, the entire hub and rotor assembly is overhung from the outlet end. The disadvantage of this type of assembly is its freedom to vibrate, particularly if resonating to the rotary motion of the shaft, and the massive hub mounting shown in the figure was designed to raise the lowest natural frequency of the assembly to a safe level.

The rotor carries 23 blades formed in fibre-glass reinforced epoxy resin, of section 10 C5/20 C50, chord 3·81 cm (1·5 inches) and aspect ratio unity. The hub/tip ratio is 0·75, space/chord ratio 0·96 at blade mid-span and the blades are mounted at a stagger angle of 34 degrees. Cascade data given in Ref. (31) suggests that such a blade row will run unloaded without encountering negative stall, the chord-based blade-relative Reynolds numbers used in the experiments being approximately 10^5. The rotor shaft is driven by a 1·5 kW (2 hp) electric motor supplied from an A.C./D.C. converter/controller: transmission is by rubber V-belt.

Microphones and probes may be inserted into the flow through a series of 1·27 cm ($\frac{1}{2}$ inch) holes drilled in the outer annulus wall and spaced axially at 15·24 cm (6 inch) intervals. At each of these positions a steel block drilled with a concentric 1·27 cm ($\frac{1}{2}$ inch) hole is attached to the casing. Further holes in these

blocks, drilled normal to the axis of the central hole, tapped and fitted with grub screws, provide a means of securing instruments in a fixed position.

The wake perturbation is introduced into the flow by means of 24 equally spaced, 1·27 cm ($\frac{1}{2}$ inch) wide strips of wire gauze, mounted radially between wooden rings and located as shown in Fig. 5. The gauze is woven from 38 SWG stainless steel wire with 50 meshes per 2·54 cm (inch), giving a screening area of 49 per cent. The determination of the wake profile is described in Section 3.5.

3.4. Instrumentation

The main-stream flow velocity and direction are measured by means of a 3·2 mm ($\frac{1}{8}$ inch) diameter cylindrical three hole probe, calibrated before use against a standard N.P.L. probe. This is located in a bush, which is in turn inserted into one of the instrument mounting blocks already described, as shown in Fig. 6. A yaw-meter is bolted to the block, and the probe is clamped in thus so that its holes are at blade mid-height. The zero angle of the yaw-meter is determined by prior measurement in a calibration tunnel with an accurately known flow direction, followed by alignment of the assembly in the same position relative to the axis of the test section. Pressure differences registered by the probe are measured on a sloping multi-tube manometer containing silicon oil, and inclined at 30 degrees to the horizontal.

The blade passing frequency (and hence rotor speed) is measured by means of a toothed disc locked to the rotor shaft outboard of the drive pulley, with 23 projections evenly spaced around its circumference. The passage of the projections activates a Dawe 3532A electromagnetic pick-up fixed to the test-section casing, feeding its signal via an impedance transformer to a Racal counter. The counter therefore gives a direct reading of blade passing frequency.

Measurements of acoustic wave amplitudes are made by means of a Bruel and Kjoer 1·27 cm ($\frac{1}{2}$ inch) condenser microphone fitted with a cathode follower and coupled to a Bruel and Kjoer type 2107 frequency analyser. The microphone is located in one of the instrument mounting blocks, with its face flush with the outer annulus wall. A visual check on the microphone signal is provided by means of a cathode ray oscilloscope, receiving the output from the frequency analyser.

3.5. Preliminary Measurements

3.5.1. *Rotor stage characteristic.* In determining the rotor characteristic a full range of operating conditions was spanned by first varying the rotor speed relative to the air supply rate, then by varying the blockage at the annulus outlet by means of wooden shutters clamped to the hub support structure. The pressure rise across the rotor was registered using 1·5 mm ($\frac{1}{16}$ inch) static tappings drilled in 1·27 cm ($\frac{1}{2}$ inch) rods, which were inserted in the instrument blocks immediately upstream and downstream of the blades. Flow velocities and directions were given by the three hole probe already described, situated for the purpose 23 cm (9 inches) downstream of the rotor, and the blade speed by the magnetic pick-up and counter.

At each operating point the axial flow velocity C_x was determined from the absolute flow velocity and angle relative to the axial direction, and the blade speed U_b, at mid-span, from the rotor speed and mean duct radius R_0. The pressures at the static tappings were displayed on the multi-tube manometer.

The complete characteristic is shown in Fig. 7.

3.5.2. *Wake perturbations.* It has already been stated that the wake perturbation downstream of the gauzes takes the form of a circumferentially sinusoidal velocity profile superimposed upon the main-stream flow. This was verified in an experiment which included a determination of the profile amplitude and axial decay rate.

The rotor assembly and duct casing were removed and the contraction outlet, complete with gauzes, was fitted with a false annular duct of the same dimensions as the test section. Slots 3 mm ($\frac{1}{8}$ inch) wide and subtending an angle of 32 degrees at the duct axis were cut in the outer casing, spaced axially at 2·54 cm (1 inch) intervals. A traverse gear carrying the three hole probe was mounted on rails so that the probe could be inserted through any one of the slots and traversed circumferentially. Each gauze occupies an angle range of 15 degrees, so the probe could be traversed through two complete periods of the wake profile.

A number of traverses was made at various air supply rates and axial stations, with the probe holes situated at annulus mid-height. It was found that the wake velocity profiles, expressed as a percentage perturbation about the mean, were independent of the mean velocity and were very closely sinusoidal. A typical result is shown in Fig. 8. The profile amplitudes were plotted against the downstream distance from the gauzes of the station at which they were measured, giving the decay curve of Fig. 9. A calculated decay curve based upon the two-dimensional mixing length theory of Schlichting[32] is also shown in the figure, and the actual decay rate is clearly rather higher than would be expected on this basis. The reason for this is not clear. Tangential velocity components introduced by the decay of the wake profile are small and were neglected.

During this experiment a number of radial traverses were made with the probe at varying axial and circumferential locations, verifying that radial and boundary layer effects were negligible.

3.6. Acoustic Experiments

3.6.1. *Unloaded blading.* This experiment was designed to test the predictions of acoustic wave amplitude given by the analysis of Section 2. Measurements were made on the downstream-going pressure wave produced by the rotor when excited by the gauze wake velocity perturbation.

The apparatus was set up as described in the foregoing sections, with the three hole probe situated 23 cm (9 inches) downstream of the rotor, its holes at annulus mid-height. Measurements were made over the widest achievable range of blade-relative Mach number by varying the rotor speed and air supply rate. For each change of Mach number the unloaded condition was found by setting the probe yaw angle to zero and noting the point at which the flow emerged axially from the rotor; there was then no transfer of tangential momentum to the flow and consequently no steady tangential blade force. Viscous effects would lead to a small axial force component and a pressure drop across the rotor, but this was ignored. At each point the barometric pressure was recorded, and the flow temperature measured by means of a thermometer inserted at the duct outlet, to enable the air density (ρ_0) and sound-speed (a) to be calculated. Flow velocities were then derived from the reading of the multi-tube manometer, and the blade speed measured using the magnetic pick-up and counter as before.

It was found that the relative outlet flow angle $\tan^{-1}(U_b/C_x)$, where U_b is the blade speed and C_x the axial flow velocity, lay always in the range 26·0 to 27·0 degrees. On this basis the flow angle and theoretical flat plate stagger angle θ, used in the analysis, was taken to be 26·5 degrees. This is equivalent to the assumption that the velocity triangles (*see* Fig. 10) scale linearly with the flow velocity, and that the frequency parameter is constant and given by equation (64). Moreover, since the interblade phase angle is predetermined by the blade-wake structure, as described in Section 3.3.1, the only variable parameter affecting sound generation is the blade-relative Mach number. The input upwash velocity normal to the theoretical aerofoil surface can also be determined, since this is given by

$$\frac{w_W}{W} = \frac{\Delta C_x}{C_x} \sin\theta \cos\theta \tag{65}$$

where ΔC_x is the amplitude of the wake velocity perturbation and the remaining symbols have their former meanings. The value of $\Delta C_x/C_x$ was obtained from Fig. 9 and gave $w_W/W = 5{\cdot}0$ per cent for this experiment.

Measurements of the pressure wave amplitudes were made using the Bruel and Kjoer microphone and frequency analyser already described. The microphone signal contained background broad-band noise, and was passed through a filter incorporated in the frequency analyser which gave a 6 per cent bandwidth at the 3 dB points when centred on blade passing frequency. The rotor speed was stable to within 0·2 per cent of its time-mean value, so the blade passing frequency was in no danger of passing outside the filter bandwidth. The frequency analyser gave a meter reading of the sound pressure level in dB relative to 0·0002 dyne/sq cm, from which the acoustic wave amplitude could be calculated. Low frequency unsteadiness in the flow gave rise to some amplitude modulation of the signal, which was counteracted by using a meter with a heavily damped motion, thereby averaging out the side-band components. The origin of this effect is discussed by Barry and Moore in Ref. (33).

Measurement of the downstream-going wave amplitude was further complicated by the presence of an additional wave travelling in the opposite direction, reflected from the duct outlet. It is shown in Appendix V that the effect of such a combination is the formation of an axial amplitude distribution with successive maxima and minima, where the distance between any adjacent pair of these is a function of the axial wavenumbers of the constituent waves. Also, the amplitude of the incident wave is the mean of the maximum and minimum values, and the amplitude of the reflected wave is one half of the difference between the two. For each operating condition, therefore, the sound pressure level was measured at each of the axially spaced instrument mounting stations, enabling the amplitude distribution to be plotted and its maxima, minima, and wavelength to be determined. The amplitude of the downstream-going wave and the ratio of reflected to incident wave amplitudes could then be calculated. These ratios, which are the reflection coefficients for the duct opening, are presented in Fig. 11; the effect of the reflected wave on the rotor excitation is discussed in Section 4.

3.6.2. *Loaded blading.* Two further experiments were performed with the rotor blades in a steadily loaded condition, in order to test the validity of the theoretical analysis when the condition of zero mean incidence is disregarded. The experimental procedure was the same as in the unloaded blading case, but it was necessary to regard the flow geometry in a slightly different way, because the main-stream flow was no longer uniform. Since the downstream-going acoustic wave was the object of the investigation, the most obvious approach was to use the outlet flow relative to the rotor as a basis for the determination of blade-relative Mach number, frequency parameter and equivalent theoretical stagger angle θ, and this is the course that was followed.

Measurements were made at two different rotor loading conditions, shown on the characteristic of Fig. 7, corresponding to $\Delta p/\frac{1}{2}\rho_0 U_b^2 = 0{\cdot}625$ and $0{\cdot}805$. These were established by presetting the yaw-meter angle and holding the absolute outlet flow angle constant. The velocity triangles, which are shown in Fig. 10, were again found to scale linearly with flow velocity, the angle θ lying in the ranges 31 to 32 and 32 to 33 degrees respectively. The input upwash perturbation was then determined using equation (65), as before.

3.6.3. *Control experiments.* The three experiments described above were repeated in the absence of an input wake perturbation, in order to confirm that the physical origin of the measured acoustic waves had been assumed correctly. The procedure was in every way similar to that already followed, except that the wake generating gauzes were removed.

3.7. Experimental Accuracy

The error associated with the main-stream velocity measurements, which were made using the sloping multi-tube manometer, depended to some extent upon the magnitude of the measured velocity itself. At low velocities the manometer levels were very steady, and the accuracy of the measurement was limited by the manometer itself. The worst error in this range was probably about 1·3 mm (0·05 inches) of silicon oil, measured on the sloping scale, representing for example at cut-off in the highly loaded case an error of approximately 3 per cent in the measured dynamic head. At high velocities unsteadiness in the manometer levels became the principal source of inaccuracy, but the greater magnitude of the measured quantities meant that the relative error introduced was no worse than the 3 per cent estimated for the low velocity case.

The combination of three hole probe and manometer was sensitive to changes in yaw angle of 5 minutes, a change which could easily be measured on the vernier yaw-meter. The greatest error here, however, was associated with the alignment of the yaw-meter relative to the duct axis, which was accurate only to about 1 degree. This was of the same order as the measured variation in the flow angle θ, and was regarded as acceptable.

Errors in the measurement of blade passing frequency and rotor speed were negligible, being substantially less than the fluctuation of the rotor speed itself. This in turn amounted to a mere 0·2 per cent variation.

By far the largest source of error in the measurements of acoustic wave amplitude was the fluctuation in this quantity introduced by flow unsteadiness, mentioned in Section 3.6.1. The meter incorporated in the

frequency analyser was heavily damped, so that this random amplitude modulation could be largely averaged out of the signal, and it was estimated that the meter could be read to within $\pm\frac{1}{2}$ dB. This represents an error of ± 6 per cent in the measured amplitude.

4. Results and Discussion

4.1. Computer Program and Theoretical Results

The calculation method described in Section 2 has been programmed in ASA Fortran for the TITAN computer in the Cambridge University Mathematical Laboratory. The program takes input values of space-chord ratio (S/C), stagger (θ), frequency parameter (λ), interblade phase angle (ϕ) and Mach number (M) and produces as output the elements of the matrix $\underline{C}$. On TITAN the time taken to compute one set of coefficients is approximately 0·1 n^2 seconds, where n is the number of points at which the upwash integral equation is satisfied, and the program requires 8 K of core store.

The accuracy of the numerical integration involved in the calculation depends heavily upon the chosen value of n. By repeating a calculation with successively higher values of n, and observing the behaviour of the calculated coefficients, the minimum n required for a desired degree of accuracy can be determined. Some examples of this process for the coefficient C_{Lb}, which is typical of the elements of matrix $\underline{C}$, and for a variety of physical conditions, are shown in Table 1. The main inferences are summarised here:

(a) For incompressible flow through a low stagger ($\theta < 60$ degrees) cascade of moderate space-chord ratio ($S/C > 1$), with a frequency parameter of about 7 or less, a value of $n = 5$ is sufficient to ensure convergence to four places of decimals.

(b) At high Mach numbers, the other conditions described above being retained, the required value of n is increased to 5. Examples are given for $M = 0{\cdot}5$ and 0·8.

(c) For cascades with high stagger and large spacing, or low stagger and small spacing, provided that the Mach number and frequency parameter are low, $n = 5$ is still sufficient.

(d) When high stagger ($\theta > 60$ degrees) is combined with small spacing ($S/C < 0{\cdot}5$) convergence deteriorates markedly. For $S/C = 0{\cdot}5$ and $\theta = 60$ degrees a value of $n = 11$ is required, and with $S/C = 0{\cdot}5$, $\theta = 75$ degrees, convergence is poor up to $n = 13$.

(e) In cases of high frequency parameter ($\lambda > 8$) convergence deteriorates, and with $\lambda = 10$, as in the examples given, is poor up to $n = 15$.

The correctness of the calculation method and program have been checked by comparison with the results of Whitehead,[24,30] Lane and Friedman[25] and Kaji and Okazaki.[17] In Table 2 lift and moment coefficients for an incompressible flow calculated by the present program are compared with results from Refs. (24) and (30). Agreement is excellent, particularly between the present method and Ref. (30), which share the same numerical computation procedure in this case. A comparison between some of the coefficients calculated for a compressible flow and those given in Refs. (24) and (25) is shown in Table 3. Here the value of $n = 3$ used by Whitehead and by Lane and Friedman is rather low for the numerical methods used in the present analysis, but agreement is very good when a value of $n = 5$ is used. In these tables the coefficients as defined in Section 2 have been divided by a factor of π in order to conform to the definitions used by the other authors.

Fig. 12 shows a comparison with results given by Kaji and Okazaki for a cascade excited by an upstream going incident acoustic wave, Ref. (17). There is excellent agreement at all points.

4.2. Comparison of Experimental Results with Theoretical Predictions

4.2.1. *Unloaded blades.* The results of the experiment performed on the unloaded rotor, together with the corresponding theoretical prediction, are shown in Fig. 13. The cut-off Mach number and acoustic wave amplitudes beyond cut-off are well predicted, but the range of Mach number obtainable with the present apparatus is small, and it is impossible to say whether or not the agreement will survive extension to higher speeds. The measurements made in the absence of the perturbation gauzes indicate that isolated rotor effects, such as the detection of blade wakes by the microphones, are negligibly small. The theoretical analysis predicts that at cut-off the acoustic wave appears with infinite amplitude, though Whitehead[24]

has shown that in this condition the energy propagating away from the rotor remains finite. In practice the cut-off point is much less clearly defined, and appreciable sound amplitudes are detected before the predicted cut-off point is reached, when the decay rate of this particular mode becomes small. The low sound levels observed well below cut-off are probably background noise.

Two further departures from ideal conditions must be mentioned here. It is assumed in the theoretical analysis that radial effects are negligible and that the flow may be regarded as two-dimensional. Tyler and Sofrin[14] have shown that each circumferential acoustic mode is made up of a series of complex radial pressure patterns, each radial mode being characterised by the number of nodes occurring in the distribution of pressure across the annulus, and although their analysis is confined to the case where there is no mean flow, essentially the same arguments with regard to radial modes apply here. In the present case only the first radial mode reaches its cut-off condition, and with the hub-tip ratio of 0·75 the radial pressure distribution for this mode is almost uniform. Neglect of radial effects in the acoustic perturbation is therefore justified. Even so, the definition of mainstream flow parameters at the duct mean radius is an approximation which must be borne in mind.

Secondly, as pointed out in Section 3, there is in addition to the downstream going wave of immediate interest an upstream going wave reflected from the duct opening. The measured reflection coefficients for the opening are shown in Fig. 11. The distance Δx between successive peaks of the axial amplitude distribution formed by superposition of the two waves was also measured, and a comparison of the values obtained with those calculated by the method of Appendix V is shown in Fig. 14. The agreement is very good except close to cut-off, where Δx is large and difficult to measure accurately. The contribution of the reflected wave to the acoustic excitation of the rotor has been ignored in the application of the theoretical analysis to the experimental case, an approximation which is good except, again, in a small region close to cut-off, where reflection coefficients for the rotor itself are large. The calculated reflection coefficients are presented in Fig. 15. Quite large differences between experiment and theory are difficult to detect in this region, because of the rapid rate of change of wave amplitude with Mach number, and elsewhere the double reflection results in a wave of much smaller amplitude than that excited by the gauze wakes.

4.2.2. *Loaded blades.* The measured and predicted wave amplitudes for the loaded rotor experiments are shown in Figs. 16 and 17. As before the cut-off Mach numbers are well predicted, but the measured wave amplitudes above cut-off are much larger than those predicted theoretically, an effect which worsens as the blade loading is increased. A possible explanation for this lies in the interaction between the incoming flow perturbations and the potential flow field about the loaded rotor blades, which leads to the formation of a distribution of quadrupole acoustic sources in the space surrounding the blade row. This phenomenon, which is raised in its fundamental form by Lighthill,[2] is described with respect to turbomachinery by Morfey.[36,37] The analysis of Section 2 does not allow for such a source distribution, taking account only of the dipole acoustic sources distributed along the blades themselves and resulting from the fluctuating blade forces. Such an explanation is not altogether convincing, however, in view of the very low Mach numbers involved; the work of Morfey[37] suggests that quadrupole sources should not be important until axial Mach numbers of approximately 0·2 are reached. The main conclusion to be drawn is that a zero loading theory is inadequate when applied to loaded blades, and a more sophisticated calculation method must be developed if this case is to be treated.

The remarks of Section 4.2.1 on isolated rotor effects and the reflected wave apply here also. Measured and theoretical values of Δx for the axial amplitude distributions are shown in Figs. 18 and 19, and agreement is again very good.

The zeros in the theoretical curves of Figs. 16 and 17 occur when the direction of wave propagation is parallel to the blade chord. Since the fluctuating forces which generate the waves are always normal to the blade chord, no sound can be radiated in this direction. The same effect is found in the curve of Fig. 13 when the Mach number scale is extended.

4.2.3. *Influence of blade speed.* Fig. 20 shows the curves of Figs. 13, 16 and 17 replotted to a scale of blade Mach number Ub/a in place of relative flow Mach number W/a. Several features emerge.

(i) All curves show approximately the same cut-off Mach number, corresponding to an interaction pattern Mach number (which is given by 23 × blade Mach number) of unity. This is a consequence of the

very low mean flow rate, which means that the cut-off condition given by Section 2.3, that is:

$$(\omega + V_\beta)^2 - (a^2 - U^2)\beta^2 > 0$$

reduces to

$$\omega^2 > a^2\beta^2 \text{ (approx.)}$$

or

$$\text{pattern Mach no.} = \frac{\omega}{a\beta} > 1.$$

This is precisely the same as the cut-off condition given by Tyler and Sofrin (14) for the zero mean flow case.

(ii) The limited range of the zero-lift experiment can be seen very clearly in this figure, and it is obviously impossible to say whether or not the experimental results for this case will diverge from the theoretical predictions, as in the loaded blade case, when the Mach number range is extended.

(iii) The discrepancy between theory and experiment increases with blade loading, so that some effect of loading is still apparent. With the low Mach numbers involved this is unlikely to be an interaction between the steady and unsteady perturbation fields, and is more probably an effect of thickness, camber and finite deflection of the mean flow, all of which are unaccounted for in the analysis but which may all affect the dipole source distribution.

5. Conclusions and Suggestions for Development

5.1. Conclusions

(a) A computer program based upon the calculation method of Section 2 enables prediction of the generation, transmission and reflection of acoustic waves by an unloaded cascade of flat plate blades, the unsteady force and moment coefficients for the blades and the strength of the shed vortex wakes, for perturbations arising from blade vibration, incident acoustic waves, and convected wake disturbances from upstream obstacles. The results obtained agree closely with force and moment coefficients calculated by Lane and Friedman[25] and Whitehead,[24] and with generated acoustic wave amplitudes predicted by Kaji and Okazaki.[17] The calculation method gives a program which is quicker in operation and smaller than that devised by Whitehead, and while similar to the method used by Kaji and Okazaki avoids much of the latter's mathematical complexity. The treatment of the kernel function singularities in the upwash integral equation is a further feature absent from the method of Ref. (17).

(b) The program is successful in predicting the acoustic wave amplitudes generated by a compressor rotor running in a duct and excited by a sinusoidal wake perturbation, provided that no steady forces act on the blades. This conclusion applies to the limited range of blade-relative Mach number obtained in the experiments to date, but nevertheless forms strong evidence that the noise generation process is correctly understood in this case. In particular the generalisation of the Kutta–Joukowski condition to unsteady flow appears to be valid up to frequency parameters of at least 3. The cut-off phonemenon and wave geometry are also well predicted.

(c) When the blades are steadily loaded the observed wave amplitudes are greater than those predicted by the theory, and this discrepancy increases with increasing loading. The cut-off Mach number and wave geometry still give good agreement between experiment and theory. A zero steady lift theory is therefore of very limited value under these circumstances.

(d) The wake velocity perturbations in the annular duct decay more rapidly than would be expected on the basis of a two-dimensional mixing length theory, even in the absence of a radial pressure gradient to incite secondary flow. This phenomenon remains to be explained, and may be important in the prediction of the noise generated by blade-wake interaction in practical turbomachines.

5.2. Further Work

As already mentioned, the Mach number range which can be obtained with the present apparatus is small, and as an immediate development it is proposed to increase this by using a more powerful air supply fan. At the same time the blade-wake geometry can be varied so that different circumferential duct modes may be studied. A further experimental possibility with a definite practical application is the operation of the blades in a stalled condition, and the investigation of the effect of stalling on sound generation.

However, the greatest need for development is in the theoretical analysis, which must be generalised to include the effect of steady blade forces. Apart from their effect on the dipole acoustic sources already considered, these forces also lead to the introduction of a number of new sound sources (Ref. (1)), in particular a quadrupole source field caused by the interaction of the potential flow around the blades with the incoming velocity perturbations. Morfey[36] has estimated the magnitude of some of these sources, demonstrating their increasing importance as the flow Mach number rises. The effect of steady blade forces is also important in the blade vibration problem, since Whitehead[38] has shown that it is only with steady lift that bending flutter can occur. A theory taking account of both steady lift and compressibility would therefore be valuable.

Some progress has been made with this problem by Whitehead,[39] who suggests a solution based upon the division of the flow into a steady uniform field, a steady perturbation field, and an unsteady perturbation field, with each component small compared with its predecessor. The relevant new sources then appear as interactions between the perturbation fields, and may be approximated by solving for each of these in the absence of the other, and combining the two to calculate the source strengths. The present calculation method would be used in the solution for the separate fields, and it is felt that its greatest initial usefulness lies in this direction.

Other developments of the theory are contemplated which, though more distant, may be no less important. Among these are the inclusion of three-dimensional effects and the acceptance as an input flow perturbation of intake or atmospheric turbulence. Finally, the treatment of transonic and supersonic machines is of increasing relevance and might usefully be considered in addition.

LIST OF SYMBOLS

a	Sound speed
a_n	Coefficients in cascade wave series
b	$\sqrt{1-M^2}$
c	Blade chord length
d	Coefficients in expansion of kernel function logarithmic singularity
$f(\eta)$	Logarithmic singularity function
l	Integer
m	Integer: blade index
n	Integer: number of points at which upwash equation is satisfied
p	Pressure perturbation: integer in Appendix I
Δp	Static pressure rise across rotor
r	Cascade wave and acoustic mode index
s	Entropy: blade spacing
t	Time
u	Velocity perturbation in x-direction
v	Velocity perturbation in y-direction
w	Upwash velocity perturbation
x	
y	Cartesian co-ordinates
Δx	Cycle length of axial amplitude distribution
z	Co-ordinate measured in direction of blade chord
$\hat{z}$	z/c
A	$\lambda^2 + \hat{\beta}^2 + 2\lambda\hat{\beta}\sin\theta$
$\underline{C}$	Matrix of output coefficients
C_L	Lift coefficient
C_M	Moment coefficient
C_x	Axial velocity
ΔC_x	Amplitude of velocity wake perturbation
F	Blade force
$K(\eta)$	Kernel function of upwash integral equation
$\underline{K}$	Kernel function matrix
M	Mach number: blade moment
N	Number of rotor blades
N_W	Number of gauze wakes
P	Acoustic pressure coefficient
R	Duct reflection coefficient
R_0	Annulus mean radius
U	Mainstream velocity in x-direction
$\underline{U}$	Upwash perturbation matrix
U_b	Blade speed at mid-span
V	Mainstream velocity in y-direction

$V(\eta)$	Function defined by equation (53)
W	Mainstream velocity $\sqrt{U^2 + V^2}$
$\underline{X}$	Matrix defined by equation (62)
Y	$\lambda M\eta/b^2$
α	Wavenumber in x-direction
$\hat{\alpha}$	αc
β	Wavenumber in y-direction
$\hat{\beta}$	βc
γ	Strength of cascade wave
δ	Angular displacement of blade
ε	Transformed chordwise co-ordinate
η	Dummy argument
θ	$\mathrm{Tan}^{-1}(V/U)$: theoretical stagger angle
λ	Frequency parameter: $\omega c/W$
ξ	Vorticity
ρ	Density perturbation
ρ_0	Mainstream density
τ	Phase angles—Appendix V
ϕ	Interblade phase angle
ψ	Transformed chordwise co-ordinate
ω	Angular frequency
Γ	Vortex strength
$\underline{\Gamma}$	Matrix of blade vorticity
Γ_w	Γ/W

Suffices—generated waves

1	Upstream pressure wave
2	Downstream pressure wave
3	Convected vorticity wave

Suffices—input perturbations and output coefficients

b	Bending vibration
δ	Torsional vibration
W	Convected wake perturbation
u	Upstream going acoustic wave
d	Downstream going acoustic wave
$-$	Denotes peak amplitude
$'$	Denotes division by Γ/S

REFERENCES

No.	*Author(s)*	*Title, etc.*
1	C. L. Morfey	A review of the sound-generating mechanisms in aircraft-engine fans and compressors. Proceedings of UTIAS/AFOSR symposium on aerodynamic noise. Toronto University Press, 1969.
2	M. J. Lighthill	On sound generated aerodynamically: I. General theory. *Proc. Roy. Soc. Series A*, Vol. 211, 1952.
3	J. E. Ffowcs-Williams and D. L. Hawkings ..	Theory relating to the noise of rotating machinery. *J. Sound Vib.*, Vol. 10, No. 1, 1969.
4	M. V. Lowson	Reduction of compressor noise radiation. *J. Acoustical Soc. of America*, Vol. 43, No. 1, 1968.
5	J. Nemec	Noise of axial fans and compressors: Study of its radiation and reduction. *J. Sound Vib.*, Vol. 6, No. 2, 1967.
6	J. Nemec	The blading of fans in its influence on noise. 4th Int. Cong. on Acoustics, Copenhagen, 1962, Paper L.52.
7	Z. Moravec	Reducing the siren noise of axial turbomachinery. *Technical Digest*, Vol. 7, No. 2, 1965.
8	M. J. T. Smith and M. E. House	Internally generated noise from gas turbine engines: Measurement and prediction. Trans. A.S.M.E., *J. Eng. for Power*, 1966.
9	N. H. Kemp and W. R. Sears	The unsteady forces due to viscous wakes in turbomachines. *J. Aero. Sci.*, Vol. 22, 1953.
10	N. H. Kemp and W. R. Sears	Aerodynamic interference between moving blade rows. *J. Aero. Sci.*, Vol. 20, No. 9, 1953.
11	R. Hetherington	Compressor noise generated by fluctuating lift resulting from rotor-stator interactions. *A.I.A.A. Journal*, Vol. 1, 1963.
12	S. L. Bragg and R. Bridge ..	Noise from turbojet compressors. *J. Roy. Aero. Soc.*, Vol. 68, No. 637, 1964.
13	I. J. Sharland	Sources of noise in axial flow fans. *J. Sound Vib.*, Vol. 1, No. 3, 1964.
14	J. M. Tyler and T. G. Sofrin ..	Axial flow compressor noise studies. *S.A.E. Trans.*, Vol. 70, 1962.
15	J. W. R. Griffiths	The spectrum of compressor noise of a jet engine. *J. Sound Vib.* (1964), 1(2), 127–140.
16	C. L. Morfey	Rotating pressure patterns in ducts, their generation and transmission. *J. Sound Vib.* 1 (1964), 60–87.
17	S. Kaji and T. Okazaki ..	Propagation of sound waves through a blade row. *J. Sound Vib.* (1970), 11(3).
18	F. O. Carta	Unsteady aerodynamic theory of a staggered cascade of oscillating airfoils in a compressible flow. U.A.C. Research Dept. Report R-0582-19, 1957.
19	F. O. Carta and R. Fauti ..	Aerodynamic interaction effects of cascaded airfoils oscillating in two-dimensional compressible flow. U.A.C. Research Dept. Report R-0582-17, 1957.
20	R. Mani	Compressibility effects in the Kemp and Sears problem. Penn State Univ. Conference, September, 1970.

21 R. Mani and G. Horvay .. Sound transmission through blade rows.
J. Sound Vib., 12, 59, 1970.

22 W. Koch .. .. .. On the transmission of sound waves through a blade row.
DFVLR-Institut fur Theoretische Gasdynamik, Aachen.

23 R. Amiet and W. R. Sears .. Reflection and transmission of oblique sound waves by a blade row.
1969 NASA SP-207, 223.

24 D. S. Whitehead .. .. Vibration and sound generation in a cascade of flat plates in subsonic flow.
Cambridge University Engineering Laboratory Report No. CUED/A-Turbo/TR 15.

25 F. Lane and M. Friedman .. Theoretical investigation of subsonic oscillating blade-row aerodynamics.
N.A.C.A. TN 4136, 1958.

26 R. Mani .. .. .. Discrete frequency noise generation from an axial flow fan blade row.
ASME Journal of Basic Engineering, March, 1970.

27 M. J. Benzakein and S. B. Kazin .. .. A theoretical prediction of aerodynamically generated noise in fans and compressors.
Paper presented at Acoust. Soc. Am., November, 1968.

28 M. J. Benzakein and S. B. Kazin .. .. Fan/compressor noise reduction.
ASME Paper 69-GY-9, March, 1969.

29 R. Mani and N. J. Lipstein .. Experimental investigation of discrete frequency noise generated by unsteady blade forces.
ASME Paper 69-WA/FE-22, 1969.

30 D. S. Whitehead .. .. Force and moment coefficients for vibrating aerofoils in cascade.
A.R.C. R. & M. No. 3254 (1960).

31 H. G. Rhoden .. .. Effects of Reynolds Number on the flow of air through a cascade of compressor blades.
A.R.C. R. & M. No. 2919 (1952).

32 H. Schlichting .. .. *Boundary layer theory.*
6th ed., McGraw-Hill Book Co. (1968).

33 B. Barry and C. J. Moore .. Subsonic fan noise.
Symposium on aerodynamic noise, Loughborough, September, 1970, Paper D.4.

34 E. G. Phillips .. .. .. Functions of a complex variable.
Oliver and Boyd, 1957.

35 Y. C. Fung .. .. .. An introduction to the theory of aeroelasticity.
John Wiley and Sons Inc., New York, 1955.

36 C. L. Morfey .. .. .. Sound generation in subsonic turbomachinery.
Trans A.S.M.E., Vol. 92D, p. 450.

37 C. L. Morfey .. .. .. Tone radiation from an isolated subsonic rotor.
Symposium on aerodynamic noise, Loughborough, September, 1970, Paper D.3.

38 D. S. Whitehead .. .. Bending flutter of unstalled cascade blades at finite deflection.
A.R.C. R. & M. 3386 (1962).

39 D. S. Whitehead .. .. Sound generation and transmission by a cascade in subsonic flow with steady lift.
Cambridge University Engineering Dept., Internal note.

APPENDIX I

Representation of a Vortex Row by a Series of Cascade Waves

If the array of vortices shown in Fig. 2 is to simulate a real rotor row then it must be cyclic in the y-direction with a period Ns, where N is the number of blades in the row. Suppose now that the array may be represented by a series of the form

$$\bar{\gamma}(y) = \sum_{n=-\infty}^{\infty} a_n \exp\left(\frac{i2\pi ny}{Ns}\right) \tag{I.1}$$

then

$$a_n = \frac{1}{Ns}\int_0^{Ns} \bar{\gamma}(y) \exp\left(-\frac{i2\pi ny}{Ns}\right) dy. \tag{I.2}$$

The function $\bar{\gamma}(y)$ may be regarded as a set of delta functions, the mth vortex being given by the function $\Gamma \exp(im\phi)\,\delta(y - ms)$, so that the contribution to the above integral from this vortex is

$$\Gamma \exp\left(im\phi - \frac{i2\pi nms}{Ns}\right).$$

Therefore,

$$\begin{aligned} a_n &= \frac{\Gamma}{Ns}\sum_{m=0}^{N-1} \exp\left(im\phi - \frac{i2\pi nm}{N}\right) \\ &= \frac{\Gamma}{Ns}\,\frac{1 - \exp(iN\phi - i2\pi n)}{1 - \exp(i\phi - 2\pi n/N)}. \end{aligned} \tag{I.3}$$

Because of the periodicity of the array, $N\phi = 2\pi p$, where p is an integer. a_n is therefore zero except when

$$(p - n) = rN \tag{I.4}$$

where r is also an integer. In this case the above expression for a_n simplifies to

$$a_n = \frac{\Gamma}{s}. \tag{I.5}$$

Substitution in equation (I.1) from equations (I.4) and (I.5) gives

$$\begin{aligned} \bar{\gamma}(y) &= \sum_{r=-\infty}^{\infty} \frac{\Gamma}{s} \exp\left\{\frac{i(p - rN)2\pi y}{Ns}\right\} \\ &= \sum_{r=-\infty}^{\infty} \frac{\Gamma}{s} \exp\left\{iy\frac{(\phi - 2\pi r)}{s}\right\}, \end{aligned}$$

which is the expression used in Section 2.5.

APPENDIX II

Relationship between Cascade Wave and Convected Vorticity Wave

Consider an element δy_0 at $y = y_0$ of the cascade wave given by

$$\gamma(y) = \frac{\Gamma}{s} \exp(i\omega t + i\beta y).$$

In a time δt_0, at $t = t_0$, this element sheds a quantity of free vorticity

$$-\frac{\Gamma}{s} i\omega \exp(i\omega t_0 + i\beta y_0)\, \delta y_0\, \delta t_0$$

which is convected downstream by a fluid element of area $U\, \delta y_0\, \delta t$. The situation is illustrated in Fig. 21. The convected vorticity wave is therefore given by

$$\xi = -\frac{i\omega\Gamma}{Us} \exp(i\omega t_0 + i\beta y_0) \tag{II.1}$$

Putting

$$t - t_0 = \frac{x}{U} \quad \text{and} \quad y - y_0 = V(t - t_0)$$

gives

$$\xi = -\frac{i\omega\Gamma}{Us} \exp\left(i\omega t - \frac{i\omega x}{U} + i\beta y - \frac{i\beta V x}{U}\right) \tag{II.2}$$

and incorporating equation (12), which states that for the convected vorticity wave

$$\omega + U\alpha + V\beta = 0,$$

we have

$$\xi = -\frac{i\omega\Gamma}{Us} \exp(i\omega t + i\alpha x + i\beta y). \tag{II.3}$$

Therefore

$$\bar{\xi} = -\frac{i\omega\Gamma}{Us} \tag{II.4}$$

which is equation (21).

APPENDIX III

Evaluation of $\sum_{r=-\infty}^{\infty} (v_3' \cos\theta - u_3' \sin\theta) \exp|(i\hat{\alpha}_3 \cos\theta + i\hat{\beta} \sin\theta)\eta|$

From equation (16) for $\hat{\alpha}_3$

$$\hat{\alpha}_3 \cos\theta + \hat{\beta} \sin\theta = -\lambda$$

which is independent of r. This term may therefore be removed from the summation.

From equations (14), (24) and (28)

$$v_3' = \frac{\lambda^2 + \hat{\beta}\lambda \sin\theta}{\lambda^2 + \hat{\beta}^2 + 2\lambda\hat{\beta} \sin\theta} \tag{III.1}$$

and

$$u_3' = \frac{\lambda\hat{\beta} \cos\theta}{\lambda^2 + \hat{\beta}^2 + 2\lambda\hat{\beta} \sin\theta}. \tag{III.2}$$

Then

$$(v_3' \cos\theta - u_3' \sin\theta) = \frac{\lambda^2 \cos\theta}{\lambda^2 + \hat{\beta}^2 + 2\lambda\hat{\beta} \sin\theta}.$$

Now $\hat{\beta} = \dfrac{\phi - 2\pi r}{(s/c)}$, so that

$$(v_3' \cos\theta - u_3' \sin\theta) = \lambda^2(s/c)^2 \cos\theta S(r) \tag{III.3}$$

where

$$\frac{1}{S(r)} = 4\pi^2 r^2 - 4\pi\left(\phi + \lambda\frac{s}{c}\sin\theta\right)r + \left(\phi^2 + \lambda^2\left(\frac{s}{c}\right)^2 + 2\lambda\phi\frac{s}{c}\sin\theta\right).$$

The required sum is $\sum_{r=-\infty}^{\infty} S(r)$. The summation is carried out by a method based upon the calculus of residues, Ref. (34), which employs the following formula:

$$\sum_{r=-\infty}^{\infty} S(r) = -\pi\{\text{The sum of the residues of } \cot \pi z S(z) \text{ at the poles of } S(z)\},$$

and the residues at these poles are

$$\mp \frac{i}{4\pi\lambda s/c \cos\theta}.$$

Inserting these values in the above summation formula gives, after some manipulation,

$$\sum_{r=-\infty}^{\infty} S(r) = \frac{1}{4\lambda s/c \cos\theta} \frac{\sinh(\lambda s/c \cos\theta)}{\sin^2\left(\dfrac{\phi}{2} + \dfrac{\lambda}{2}\dfrac{s}{c}\sin\theta\right) + \sinh^2\left(\dfrac{\lambda}{2}\dfrac{s}{c}\cos\theta\right)}. \tag{III.4}$$

Finally, incorporating equations (I.12) and (I.13) we have

$$\sum_{r=-\infty}^{\infty} (v_3' \cos\theta - u_3' \sin\theta) \exp|(i\hat{\alpha}_3 \cos\theta + i\hat{\beta} \sin\theta)\eta|$$
$$= \frac{\lambda}{4}\frac{s}{c}\left|\frac{\sinh(\lambda s/c \cos\theta)}{\sin^2\left(\dfrac{\phi}{2} + \dfrac{\lambda}{2}\dfrac{s}{c}\sin\theta\right) + \sinh^2\left(\dfrac{\lambda}{2}\dfrac{s}{c}\cos\theta\right)}\right| \exp(-i\lambda\eta),$$

which is equation (43).

APPENDIX IV

Kernel Function Singularities

The singularities in the kernel function of equation (30) appear because the velocities induced at the point $\hat{z}$ on the reference blade by the vorticity at this same point are infinite. The remaining blades in the cascade can give rise to non-singular terms only. Consequently in the extraction of the singularities, the reference blade may be treated as though it were an isolated aerofoil.

Fung[35] gives an expression for the kernel function for such an aerofoil. With adapted notation this is

$$K(\eta) = -\frac{\lambda}{4b}\exp(iMY)iM\frac{Y}{|Y|}H_1^{(2)}(|Y|) - H_0^{(2)}(|Y|)$$
$$-\frac{i\lambda b}{4}\exp(-i\lambda\eta)\frac{2}{\pi b}\log\frac{1+b}{M} + \int_0^{Y/M}\exp(iu)H_0^{(2)}(M|u|)\,du \qquad \text{(IV.1)}$$

where

$$b = \sqrt{1-M^2}$$

and

$$Y = \frac{\lambda M}{b^2}\eta$$

$H_0^{(2)}$ and $H_1^{(2)}$ are Hankel functions of the second kind, order 0 and 1 respectively.

Expanding the Hankel functions and discarding terms which do not involve $\log|Y|$ or Y^{-1} gives

$$K(\eta) = -\frac{\lambda}{4b}\exp(iMY)\left\{iM\frac{Y}{|Y|}\left(\frac{i2}{\pi|Y|} - \frac{i2}{\pi}J_1|Y|\log|Y|\right) + \frac{2i}{\pi}J_0|Y|\log|Y|\right\}$$
$$-\frac{i\lambda b}{4}\exp(-i\lambda\eta)\left\{\frac{2}{\pi b}\log\frac{1+b}{M} + \int_0^{Y/M}\exp(iu)\left(-\frac{2i}{\pi}\right)J_0|Mu|\log|Mu|\,du\right\}. \qquad \text{(IV.2)}$$

The term $-\frac{\lambda}{4b}\exp(iMY)\left|iM\frac{Y}{|Y|}\left(\frac{2i}{\pi|Y|}\right)\right|$ may be separated from this expression. It forms the non-logarithmic singularity mentioned in Section 2.11, that is

$$\frac{\sqrt{1-M^2}\exp(iM^2\lambda\eta/(1-M^2))}{2\pi\eta}.$$

Furthermore it is easily shown that as $M \to 0$ (η finite) the terms involving $\log|M|$ cancel, so that there is no singularity at $M = 0$. Subtracting out these terms we are left with

$$K(\eta) = -\frac{\lambda}{2\pi b}\exp(iMY)\log\left|\frac{Y}{M}\right|\{MJ_1(Y) + iJ_0(Y)\}$$
$$-\frac{\lambda b}{2\pi}\exp(-i\lambda\eta)\int_0^{Y/M}\exp(iu)J_0(Mu)\log|u|\,du. \qquad \text{(IV.3)}$$

Putting

$$d\chi = \exp(iu)J_0(Mu)\,du$$
$$\chi = \int_0^u \exp(ix)J_0(Mx)\,dx,$$

the integral may be written

$$\int_0^{Y/M}\exp(iu)J_0(Mu)\log|u|\,du = \left|\chi\log|u|\right|_0^{Y/M} - \int_0^{Y/M}\frac{\chi}{u}\,du.$$

Now $d\chi$ can be expanded as follows

$$d\chi = 1 + c_1 u + c_2 u^2 + \text{etc.}$$

where c_1, c_2, etc. are constants. Therefore

$$\chi = u + \tfrac{1}{2} c_1 u^2 + \text{etc.},$$

$$\chi \log |u| \to 0 \quad \text{as} \quad u \to 0$$

and $\int_0^{Y/M} (\chi/u)\, du$ becomes a power series in Y/M.

Once again discarding non-logarithmic terms, we have finally

$$K(\eta) = -\frac{\lambda}{2\pi b} \log \left| \frac{Y}{M} \right| \left| \exp(iMY)\{MJ_1(Y) + iJ_0(Y)\} + b^2 \exp(-i\lambda\eta) \int_0^{Y/M} \exp(iu) J_0(Mu)\, du \right| \quad \text{(IV.4)}$$

where the expression multiplying $\log |Y/M|$ is the $f(\eta)$ of Section 2.11. This function may be expanded as a power series of the form

$$f(\eta) = -\frac{\lambda}{2\pi b}(d_0 + d_1\eta + d_2\eta^2 + \text{etc.}), \quad \text{(IV.5)}$$

the integration being carried out term by term. Only the first term in the expansion becomes infinite at $\eta = 0$ when multiplied by $\log |\eta|$, but it is necessary to retain some of the others in the formula of equation (46) as these are handled badly by the trapezoidal rule. It is found by trial, however, that no significant increase in accuracy results from taking terms of higher order than η^3. The required coefficients are

$$\begin{aligned} d_0 &= i \\ d_1 &= \left(1 - \frac{M^2}{2b^2}\right)\lambda, \\ d_2 &= -i\left(1 - \frac{1}{2b^2} + \frac{M^2}{4b^4}\right)\lambda^2 \end{aligned} \quad \text{(IV.6)}$$

and

$$d_3 = -\frac{1}{2}\left(1 - \frac{1}{b^2} + \frac{M^2}{6b^4} + \frac{1}{3b^4} - \frac{3}{8}\frac{M^4}{b^6} + \frac{M^6}{6b^6}\right)\lambda^3.$$

APPENDIX V

Effect of Reflected Wave on Duct Measurements

When a reflected wave is present in the duct the net pressure perturbation at a point is given by adding together the effects of one wave of downstream-going type and one of upstream-going type. At a fixed circumferential location we have

$$p = \bar{p}\cos(\omega t + \alpha_2 x + \tau_2) + R\bar{p}\cos(\omega t + \alpha_1 x + \tau_1)$$

where $\bar{p}$ is the amplitude of the downstream-going wave, R is the reflection coefficient of the duct opening, τ_1 and τ_2 are fixed phase angles, and α_1 and α_2 are the wavenumbers defined by equation (11). With some manipulation this expression may be re-written as

$$p = \bar{p}|(1 + R^2) + 2R\cos\{(\alpha_2 - \alpha_1)x + 2\tau_2'\}|^{\frac{1}{2}}$$
$$\times \cos\left|\omega t + \frac{\alpha_2 + \alpha_1}{2}x + \tau_1' + \tan^{-1}\left(\frac{1 - R}{1 + R}\tan\frac{\alpha_2 - \alpha_1}{2}x + \tau_2'\right)\right|$$

where

$$\tau_2' = \frac{\tau_2 - \tau_1}{2}, \qquad \tau_1' = \frac{\tau_2 + \tau_1}{2}.$$

The amplitude of the combined perturbation therefore fluctuates between $\bar{p}(1 + R)$ and $\bar{p}(1 - R)$, so that both $\bar{p}$ and R may be determined from a knowledge of the maximum and minimum values of this amplitude. In addition the distance between two successive maxima or minima is given by

$$\Delta x = \frac{2\pi}{\alpha_2 - \alpha_1}$$

and this can be calculated using equation (11).

TABLE I

Convergence of Numerical Solution

$\frac{s}{c}$	θ	λ	ϕ	M	n	C_{Lb}	
						Real	Imaginary
1·0	0·0	1·0	π	0·0	4	2·7504	−0·0507
					5	2·7505	−0·0507
					6	2·7505	−0·0507
3·8	0·0	1·4	π	0·5	5	1·0901	−1·4515
					6	1·0902	−1·4515
					7	1·0902	−1·4515
1·0	30°	0·631	$\frac{\pi}{2}$	0·8	5	1·0263	−0·7685
					6	1·0264	−0·7684
					7	1·0264	−0·7684
0·25	0·0	1·0	0·1	0·2	5	0·3773	0·1968
					6	0·3774	0·1970
					7	0·3774	0·1970
1·0	60°	1·0	π	0·1	4	2·5683	−0·1070
					5	2·5682	−0·1071
					6	2·5682	−0·1071
0·5	60°	1·0	π	0·1	10	5·3658	−0·5790
					11	5·3659	−0·5790
					12	5·3659	−0·5790
1·0	75°	1·0	π	0·1	5	2·2613	0·0649
					6	2·2613	0·0649
					7	2·2613	0·0649
0·5	75°	1·0	π	0·1	11	5·0914	12·9404
					12	5·1350	13·0203
					13	5·1430	13·0349
1·59	0	10·0	π	0·18	13	1·6249	−8·8657
					14	1·6250	−8·8661
					15	1·6254	−8·8669
0·5	75°	10·0	π	0·1	13	5·1428	13·0349
					14	5·1380	13·0238
					15	5·1439	13·0336

TABLE 2

Comparison with Incompressible Results

Freq. Par. = 2·0, $M = 0$, $s/c = 1{\cdot}0$, $n = 4$

$\theta = 0$, $\phi/2\pi = 0{\cdot}5$

		Bending		Torsion		Wakes	
C_L	a	−0·7303	−0·3820	−0·4834	−1·4372	−0·3245	0·3743
	b	−0·7318	−0·3817	−0·4409	−1·4382	−0·3249	0·3752
	c	−0·7317	−0·3816	−0·4407	−1·4373	−0·3248	0·3752
C_M	a	−0·2026	−0·2362	0·0408	−0·6594	−0·0900	0·1038
	b	−0·2035	−0·2362	0·0395	−0·6602	−0·0903	0·1043
	c	−0·2037	−0·2361	0·0385	−0·6598	−0·0903	0·1044

$\theta = 45°$, $\phi/2\pi = 0{\cdot}5$

		Bending		Torsion		Wakes	
C_L	a	−0·6840	−0·3160	−0·4673	−1·3036	−0·2680	0·3548
	b	−0·6796	−0·3180	−0·4596	−1·3020	−0·2671	0·3518
	c	−0·6795	−0·3181	−0·4595	−1·3017	−0·2672	0·3517
C_M	a	−0·1903	−0·2073	0·0197	−0·6015	−0·0745	0·0988
	b	−0·1875	−0·2080	0·0239	−0·5998	−0·0737	0·0971
	c	−0·1876	−0·2081	0·0233	−0·5997	−0·0737	0·0970

$\theta = 75°$, $\phi/2\pi = 0{\cdot}8$

		Bending		Torsion		Wakes	
C_L	a	−0·2841	−0·3792	0·0309	−0·7971	−0·2806	0·0116
	b	−0·2686	−0·3821	0·0428	−0·7822	−0·2741	−0·0064
	c	−0·2686	−0·3823	0·0429	−0·7819	−0·2741	−0·0065
C_M	a	−0·0757	−0·2210	0·1598	−0·4561	−0·0710	0·0066
	b	−0·0685	−0·2264	0·1658	−0·4573	−0·0661	−0·0050
	c	−0·0685	−0·2264	0·1652	−0·4570	−0·0658	−0·0049

Note. a = Ref. (24), b = Ref. (30), c = present program.
For each coefficient first the real part then the imaginary part is shown on the same line.

TABLE 3

Comparison with Compressible Results

$s/c = 3{\cdot}8$; $\theta = 0$; $\phi/2\pi = 0{\cdot}5$; $M = 0{\cdot}5$

$\lambda = 1{\cdot}0$

		Bending		Torsion	
C_L	a	−0·7212	0·0665	−0·8277	−0·0866
	b	−0·7200	0·0672	−0·8266	−0·0856
	c	−0·7178	0·0684	−0·8213	−0·0807
	d	−0·7191	0·0672	−0·8236	−0·0840
C_M	a	0·1509	−0·1051	0·1826	−0·1496
	b	0·1506	−0·1052	0·1824	−0·1497
	c	0·1497	−0·1038	0·1795	−0·1471
	d	0·1509	−0·1045	0·1824	−0·1483

$\lambda = 1{\cdot}2$

		Bending		Torsion	
C_L	a	−0·7546	0·0962	−0·9137	−0·0660
	b	−0·7538	0·0959	−0·9127	−0·0664
	c	−0·7458	0·0978	−0·8966	−0·0576
	d	−0·7502	0·0960	−0·9048	−0·0634
C_M	a	0·1323	−0·1301	0·1733	−0·1964
	b	0·1323	−0·1300	0·1733	−0·1961
	c	0·1305	−0·1263	0·1675	−0·1894
	d	0·1328	−0·1288	0·1734	−0·1934

$\lambda = 1{\cdot}4$

		Bending		Torsion	
C_L	a	−0·3383	0·4648	−0·5077	0·5073
	b	−0·3433	0·4670	−0·5158	0·5077
	c	−0·3491	0·4550	−0·5100	0·4882
	d	−0·3470	0·4620	−0·5147	0·4997
C_M	a	−0·0303	−0·1167	−0·0319	−0·2319
	b	−0·0306	−0·1180	−0·0310	−0·2344
	c	−0·0291	−0·1165	−0·0241	−0·2295
	d	−0·0269	−0·1198	−0·0257	−0·2328

Note. a = Ref. (24); b = Ref. (25); c = present program, $n = 3$; d = present program, $n = 5$.

For each coefficient first the real part then the imaginary part is shown on the same line.

Coefficients are referred to an axis position at the mid-chord point.

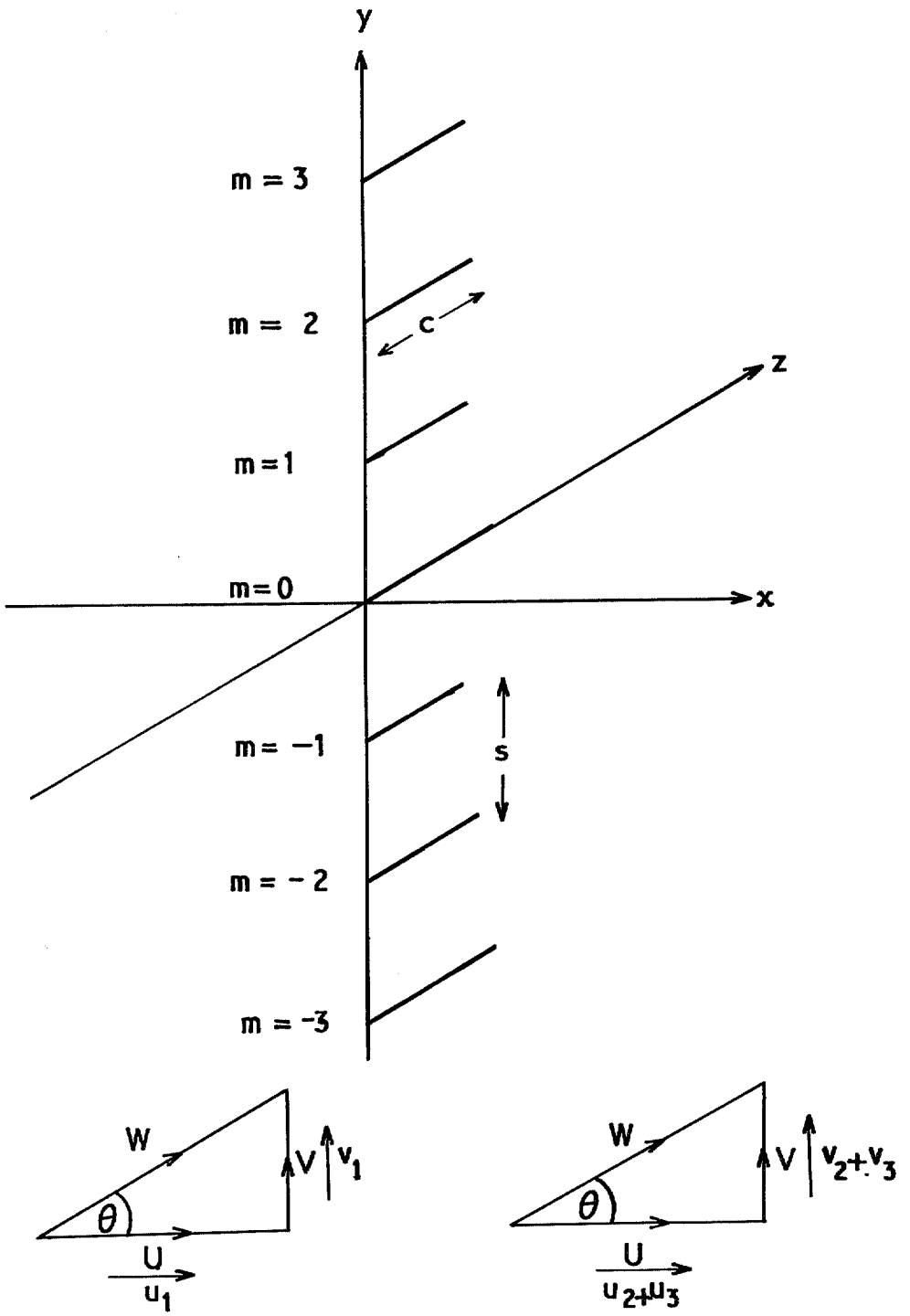

FIG. 1. Cascade model.

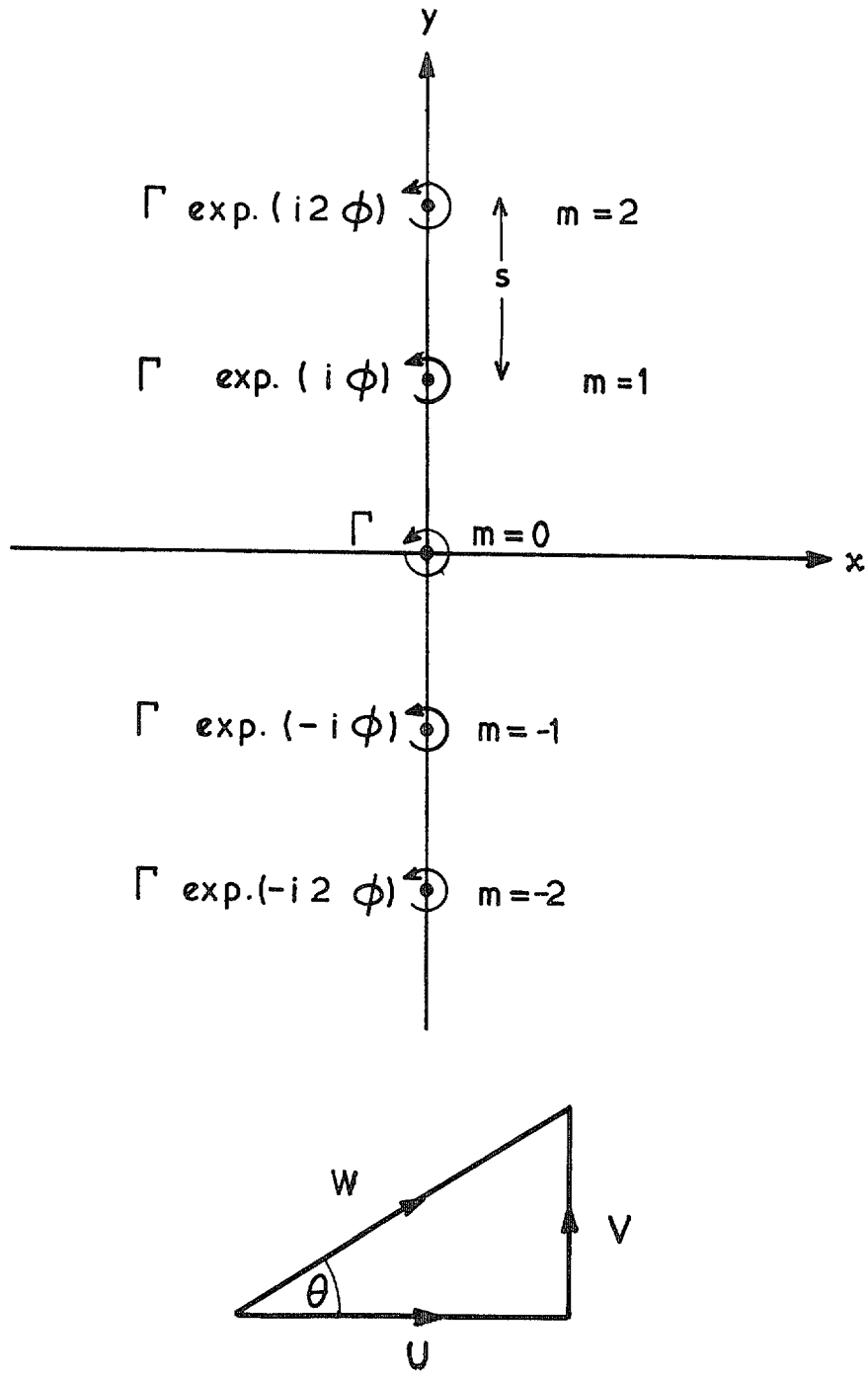

FIG. 2. Vortex row.

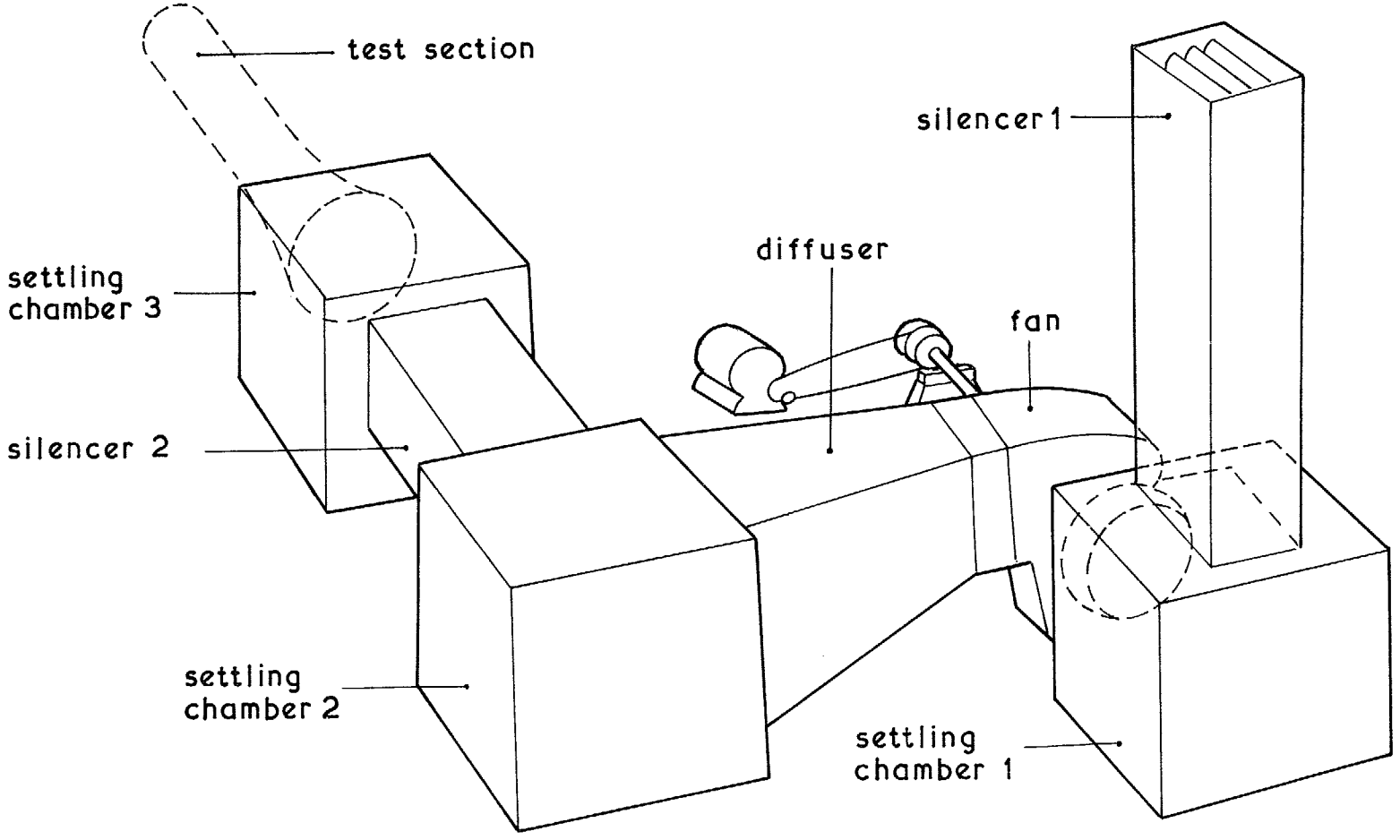

FIG. 3. Overall layout of apparatus.

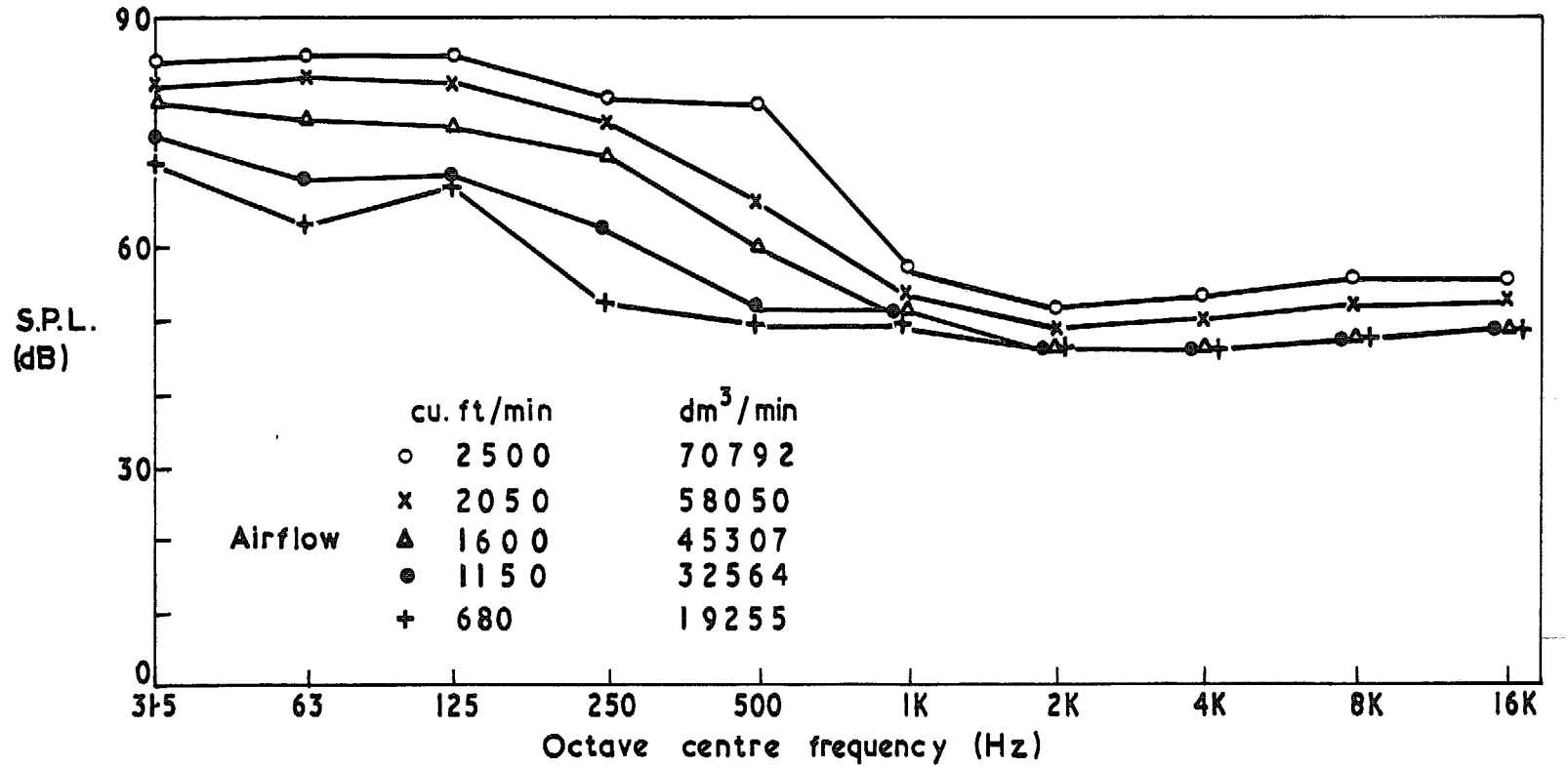

FIG. 4. Background noise levels.

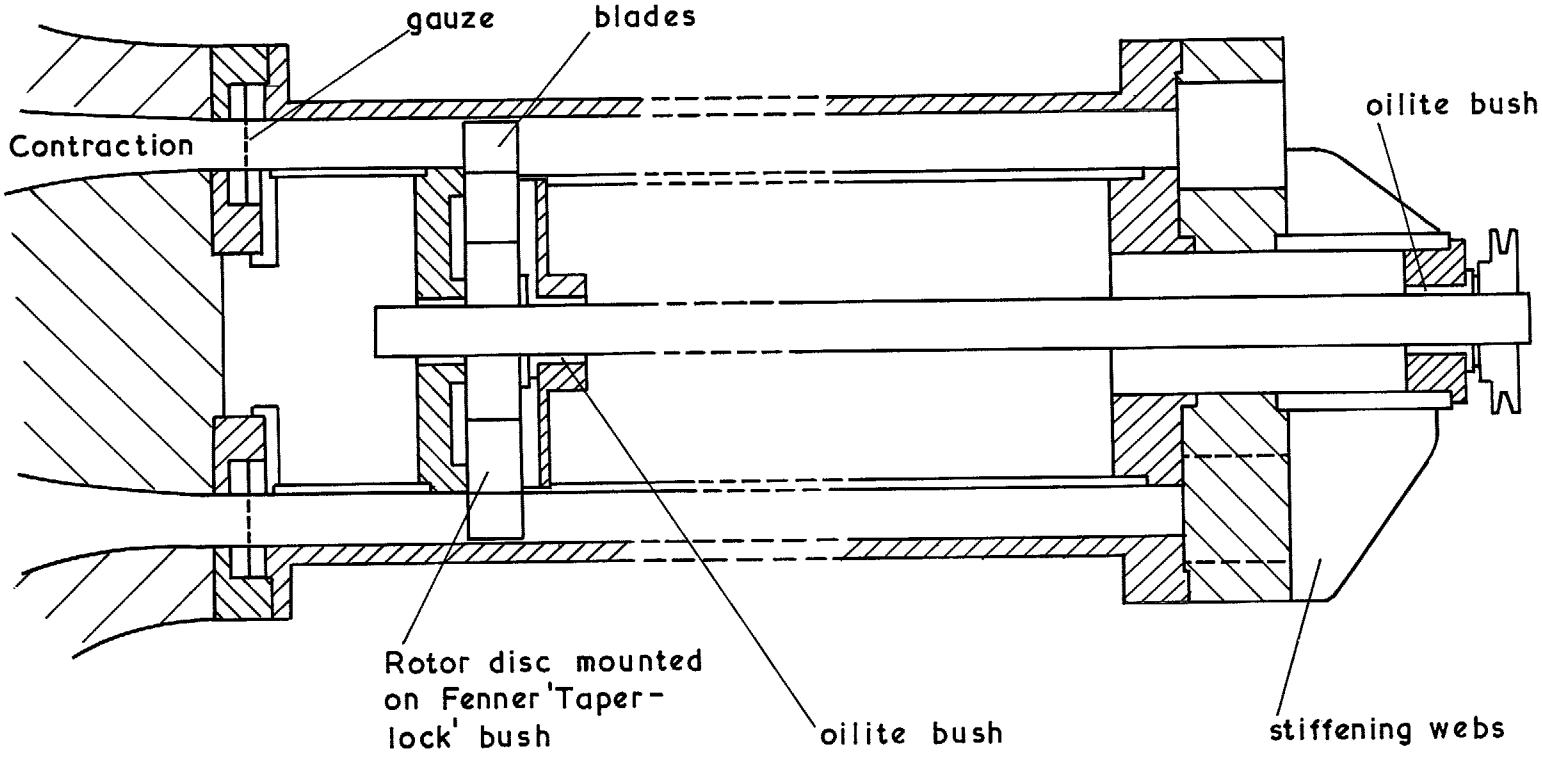

FIG. 5. Test section—construction.

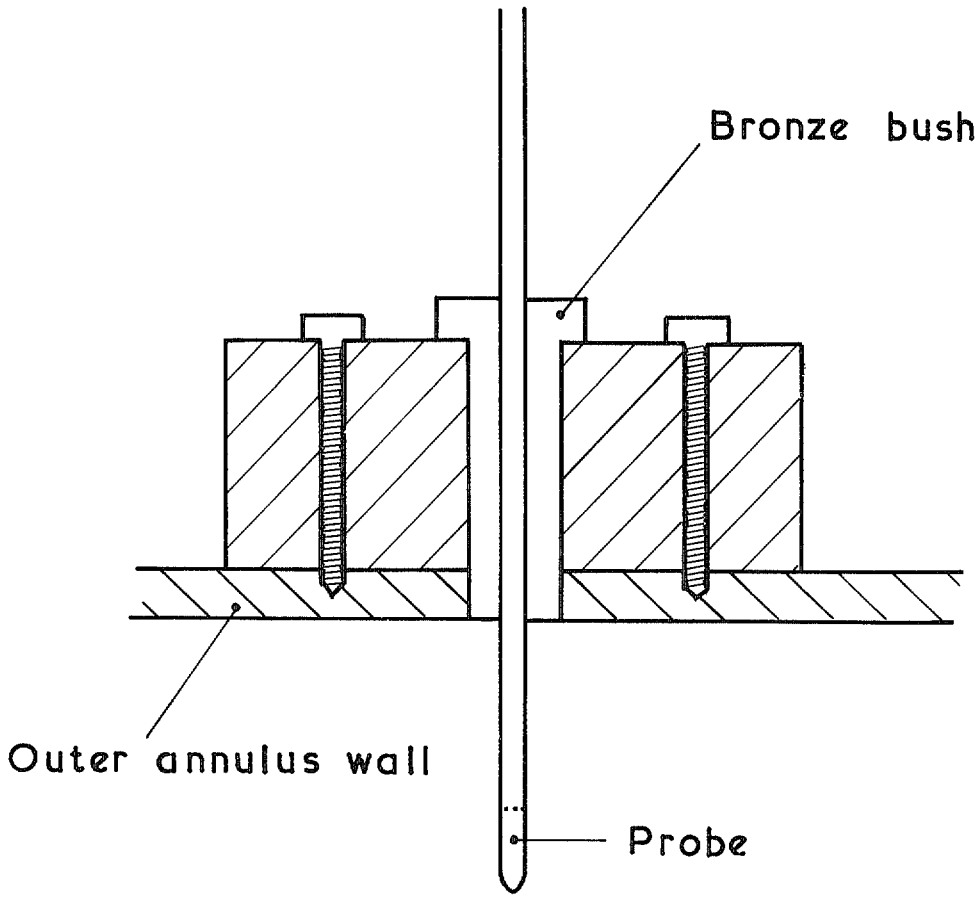

FIG. 6. Instrument mounting detail.

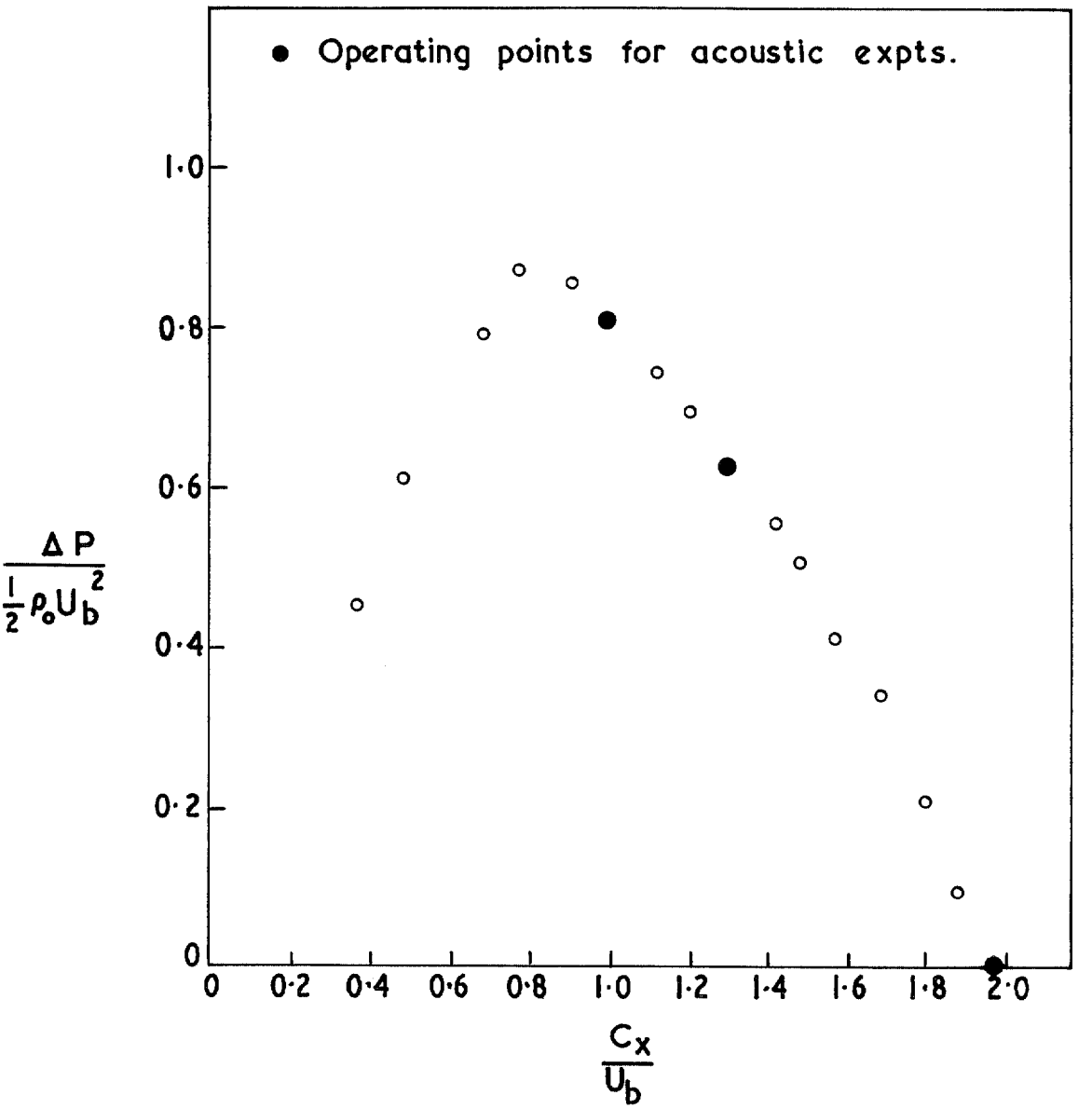

FIG. 7. Rotor stage characteristic.

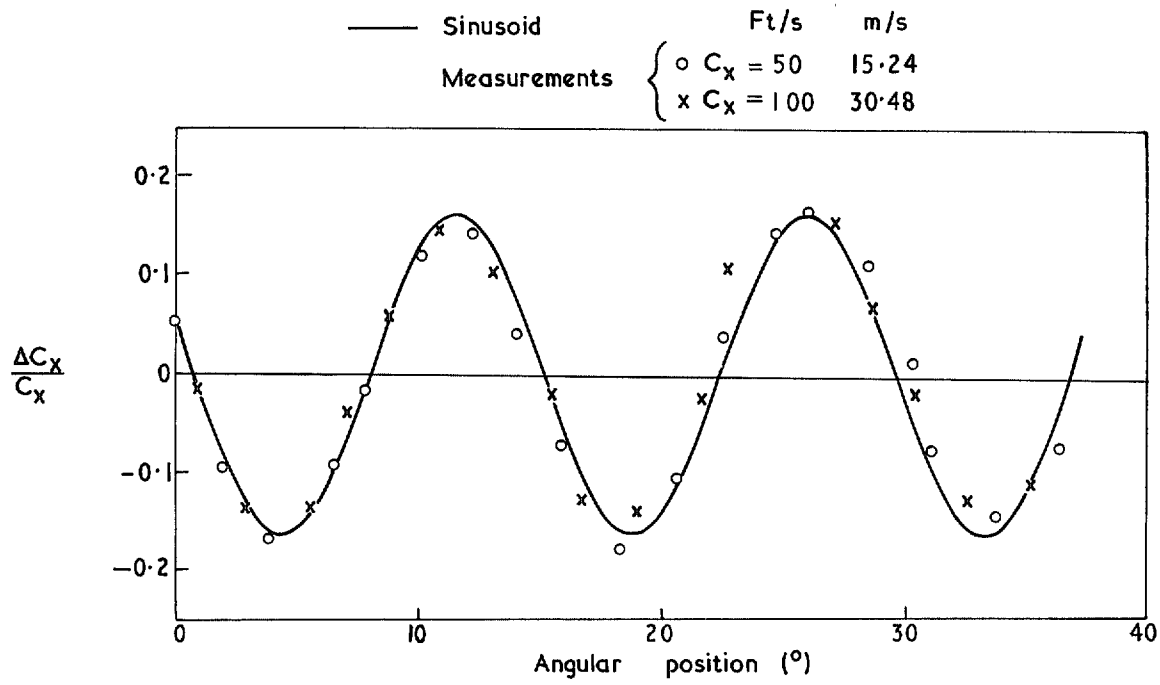

FIG. 8. Wake velocity profile 13·2 cm (5·2 inches) downstream of gauzes.

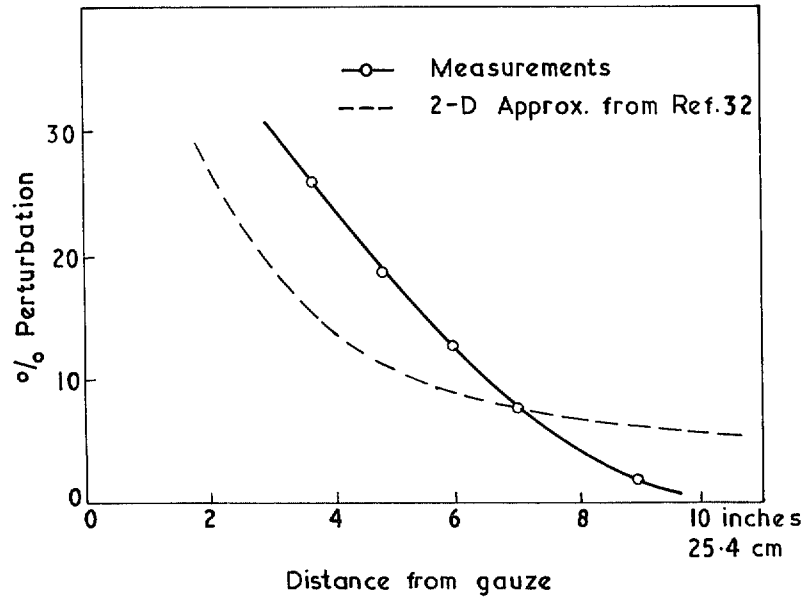

FIG. 9. Wake decay rate.

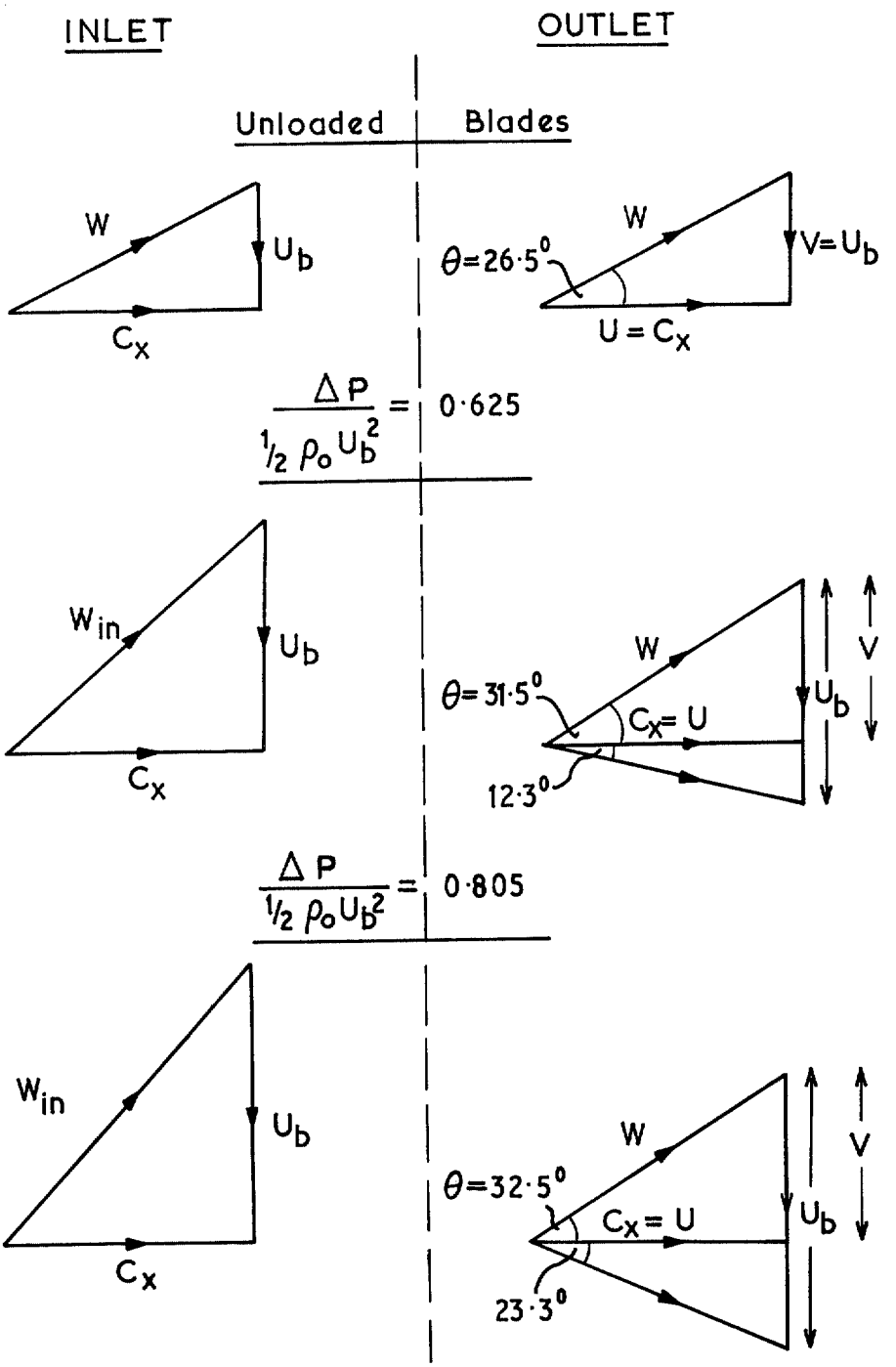

FIG. 10. Rotor velocity triangles.

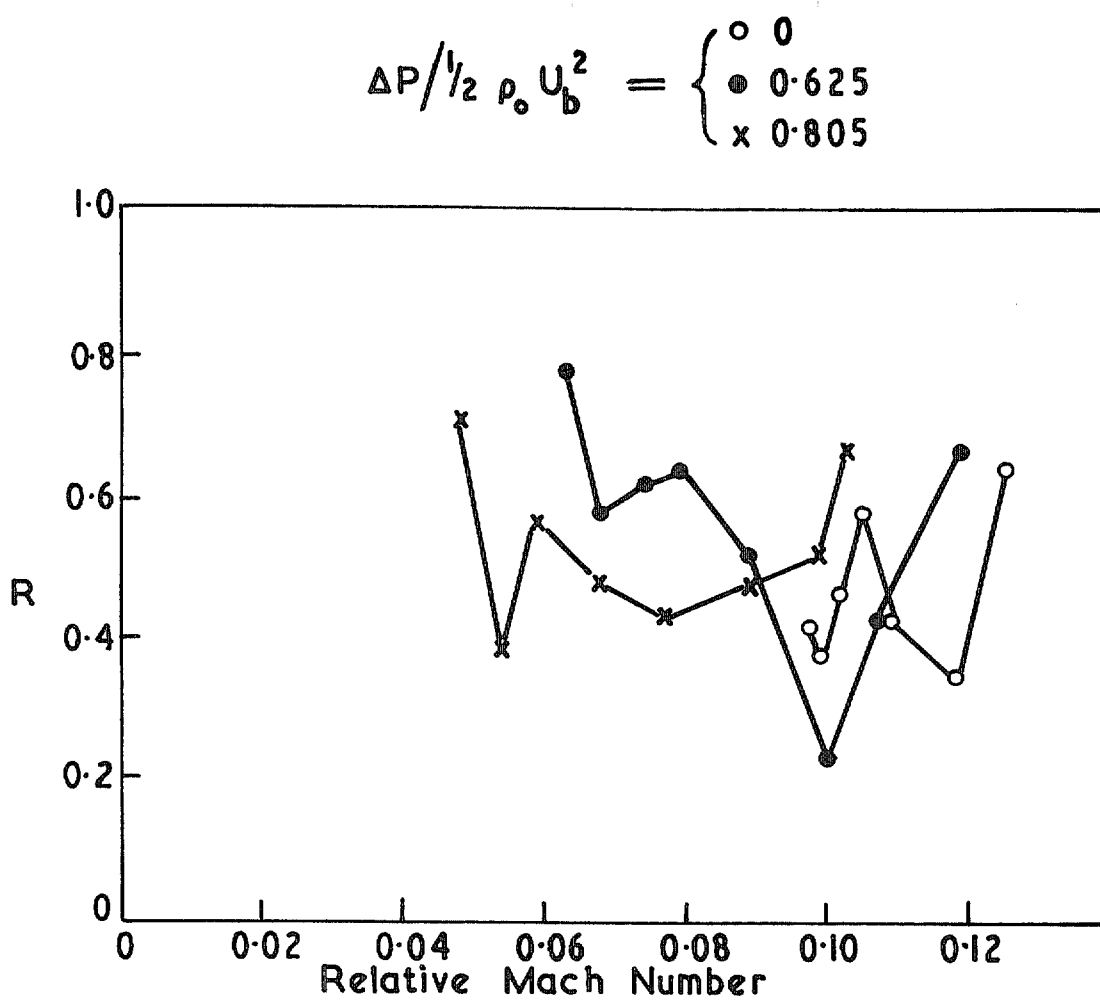

FIG. 11. Duct reflection coefficients.

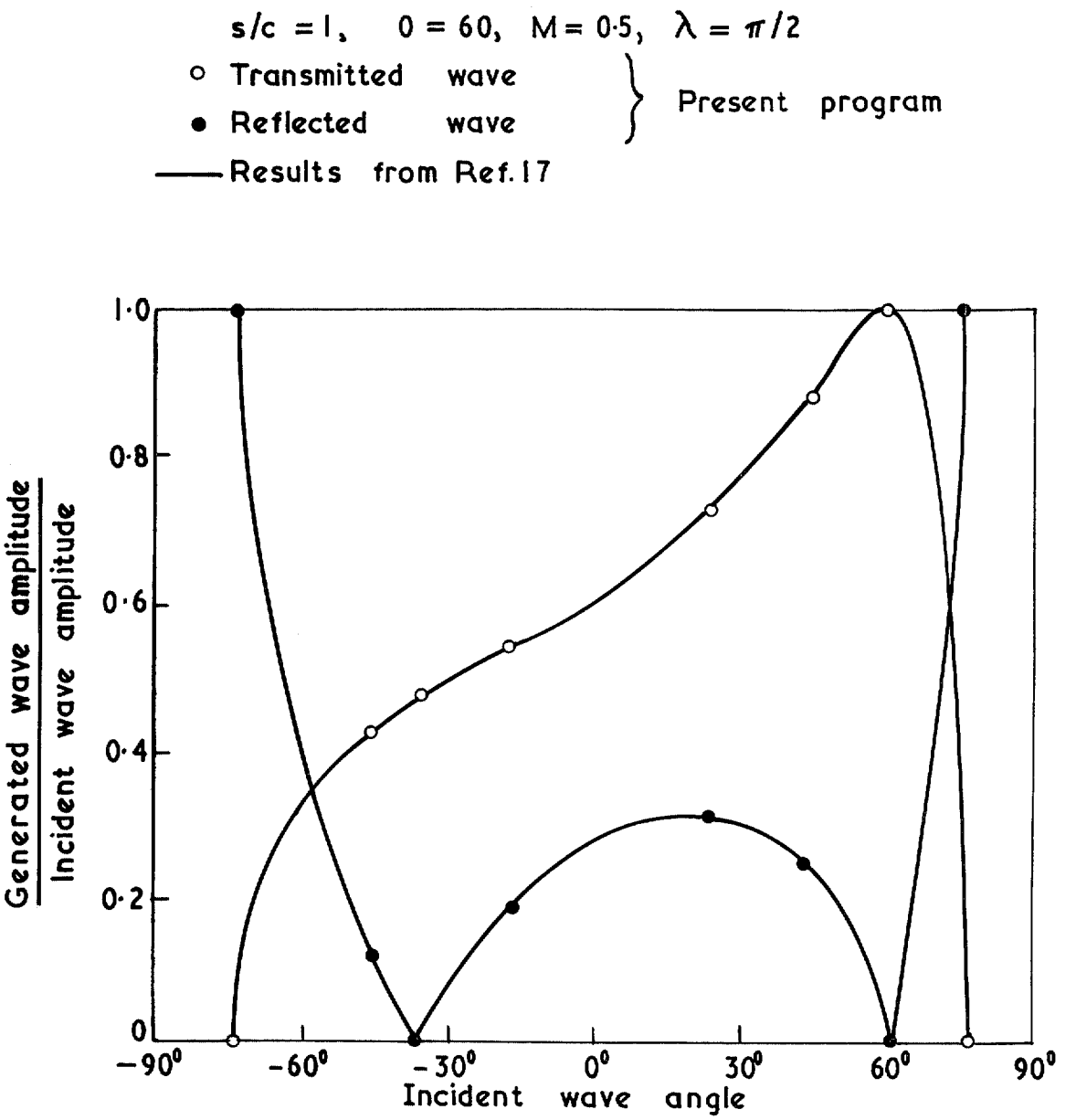

FIG. 12. Comparison with Kaji and Okazaki. Upstream going incident wave.

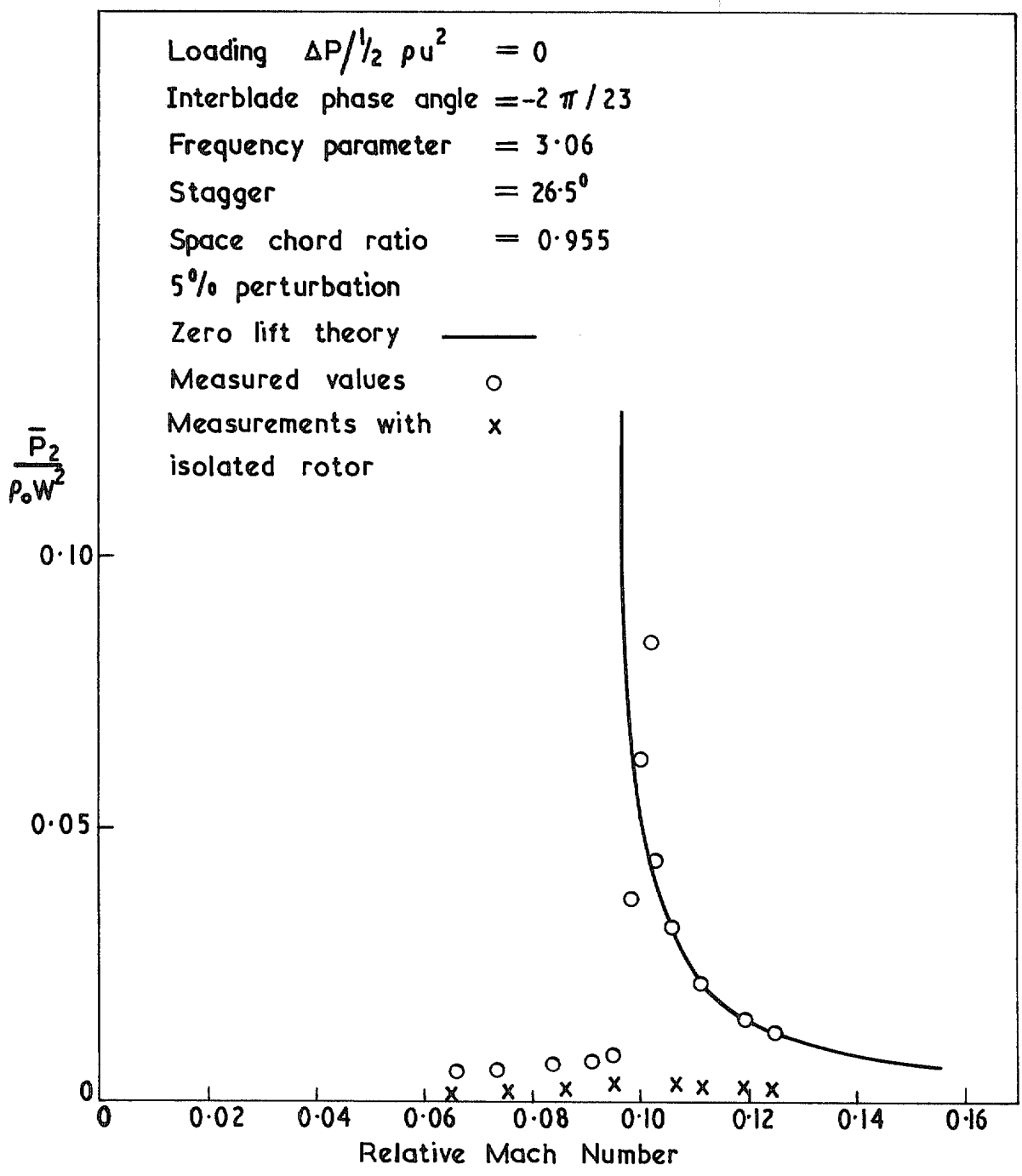

FIG. 13. Downstream acoustic wave.

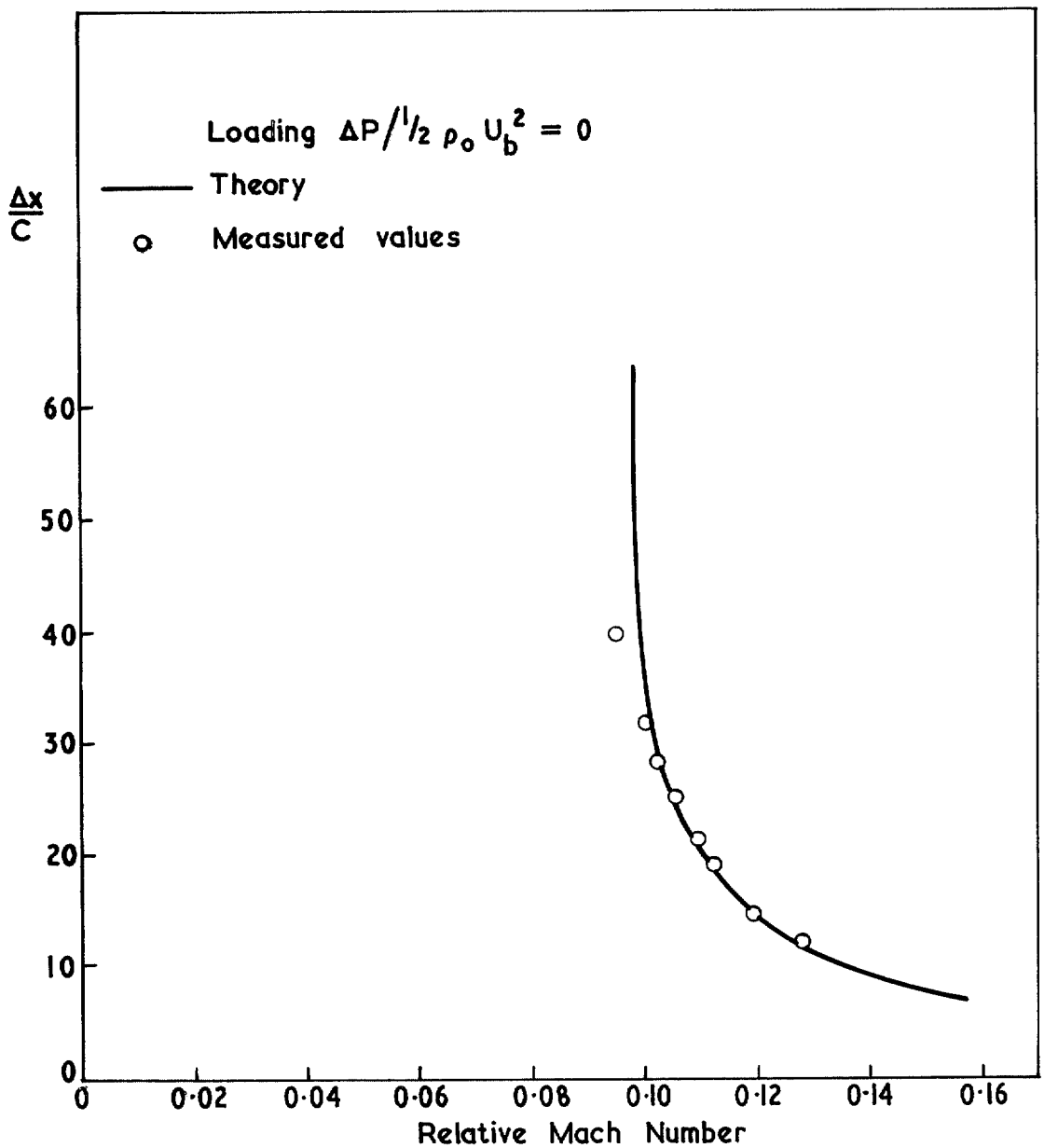

FIG. 14. Axial amplitude distribution cycle-length.

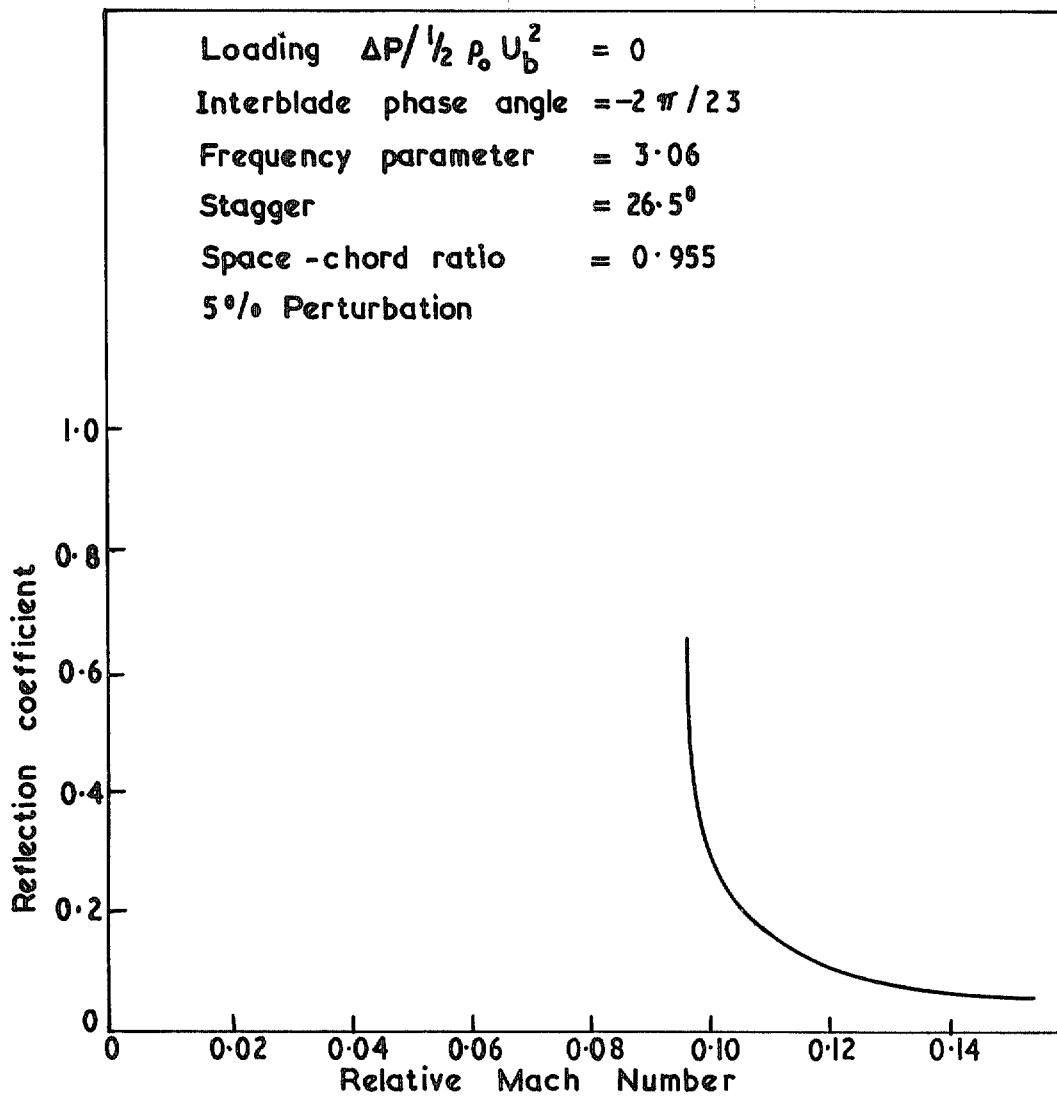

FIG. 15. Rotor reflection coefficients. Upstream going incident wave.

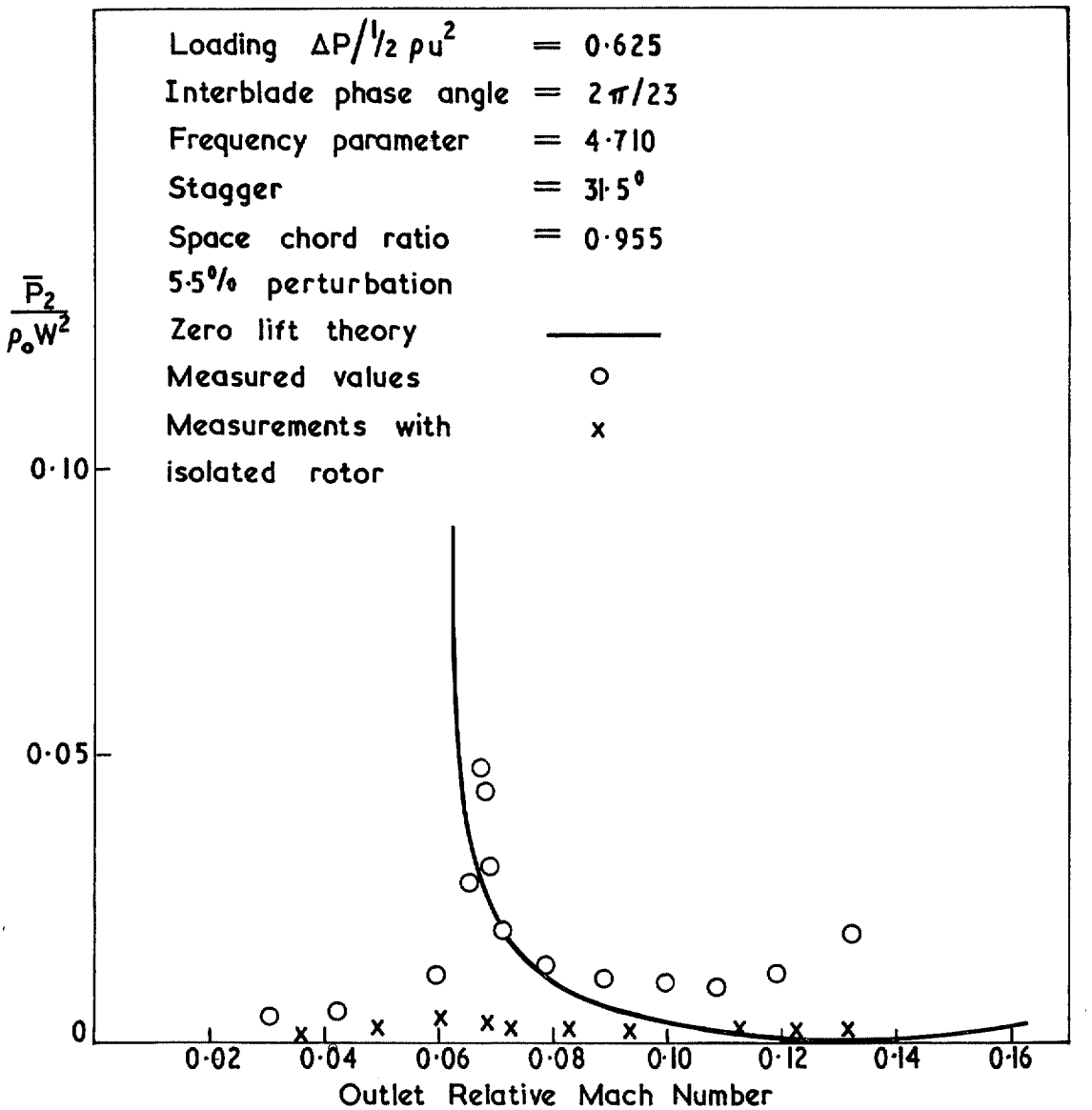

FIG. 16. Downstream acoustic wave.

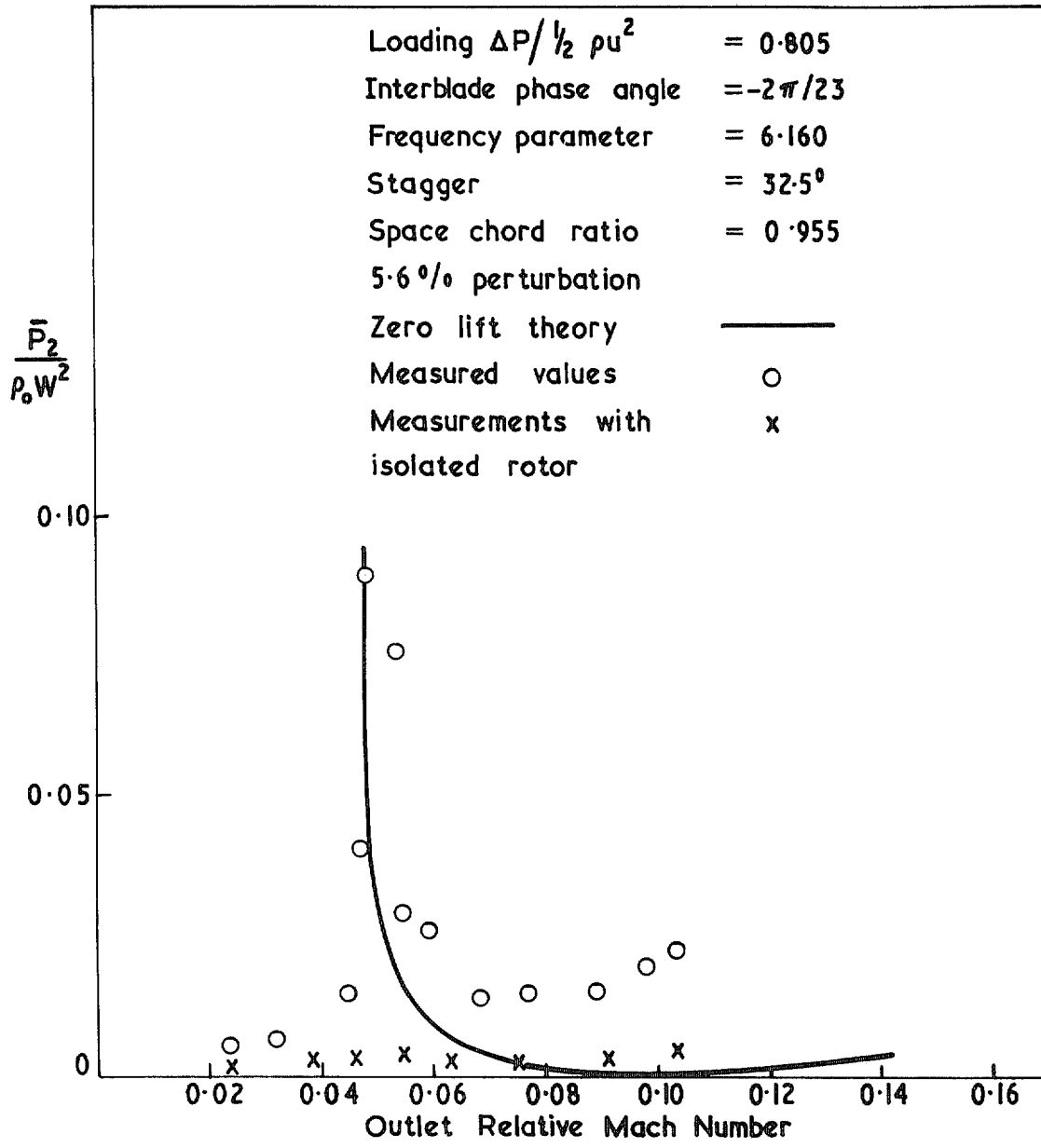

FIG. 17. Downstream acoustic wave.

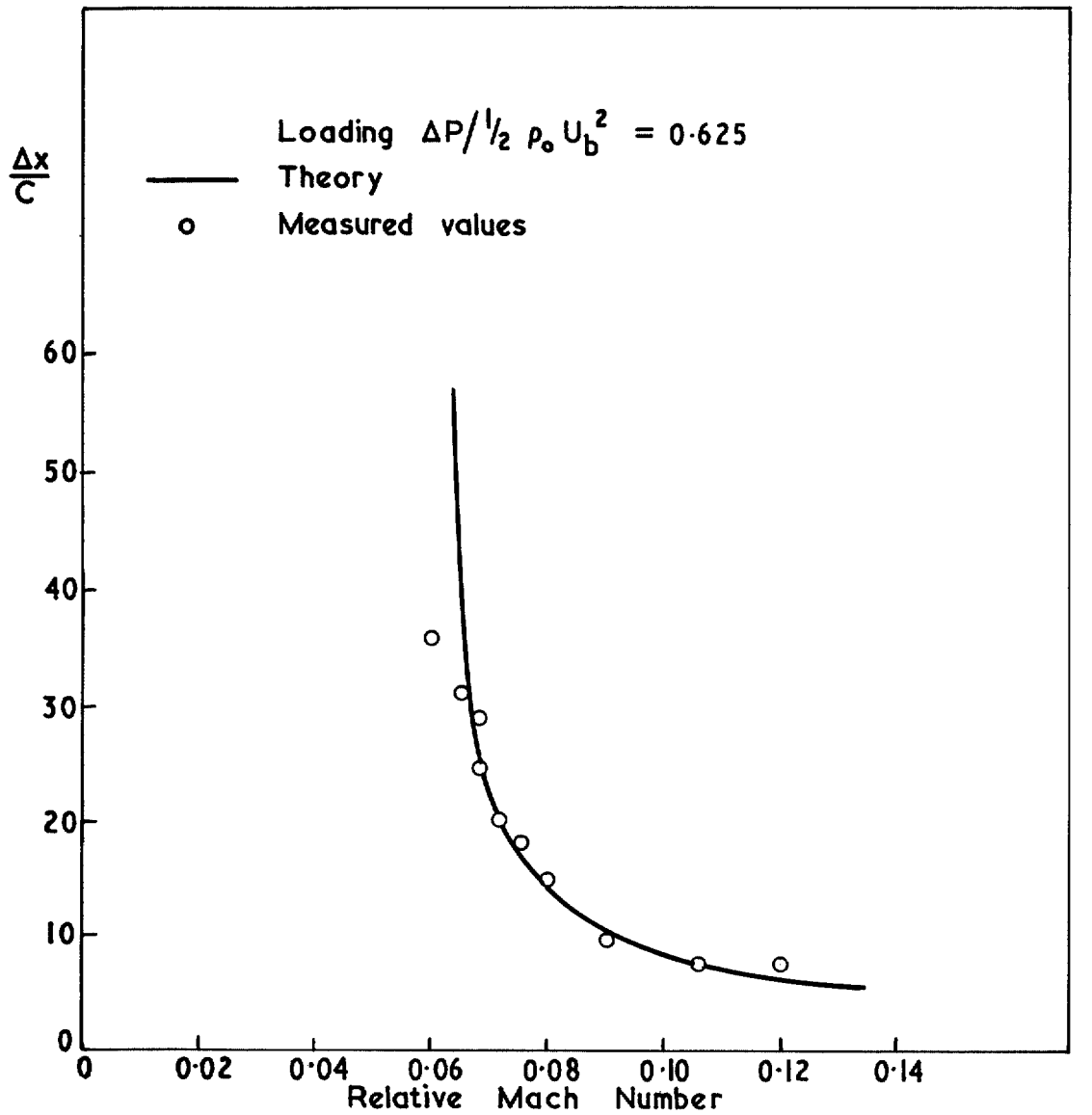

FIG. 18. Axial amplitude distribution-cycle length.

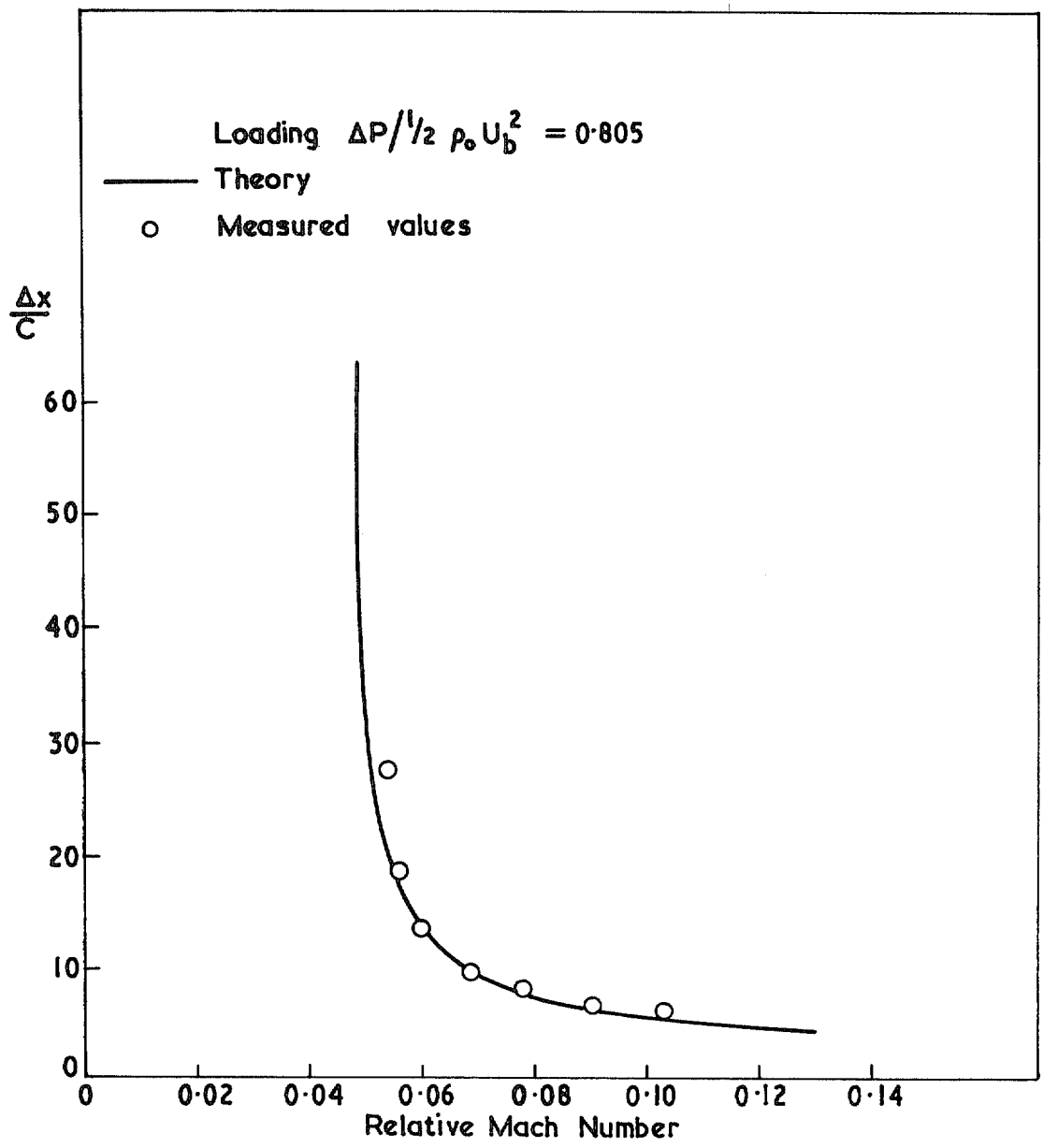

FIG. 19. Axial amplitude distribution-cycle length.

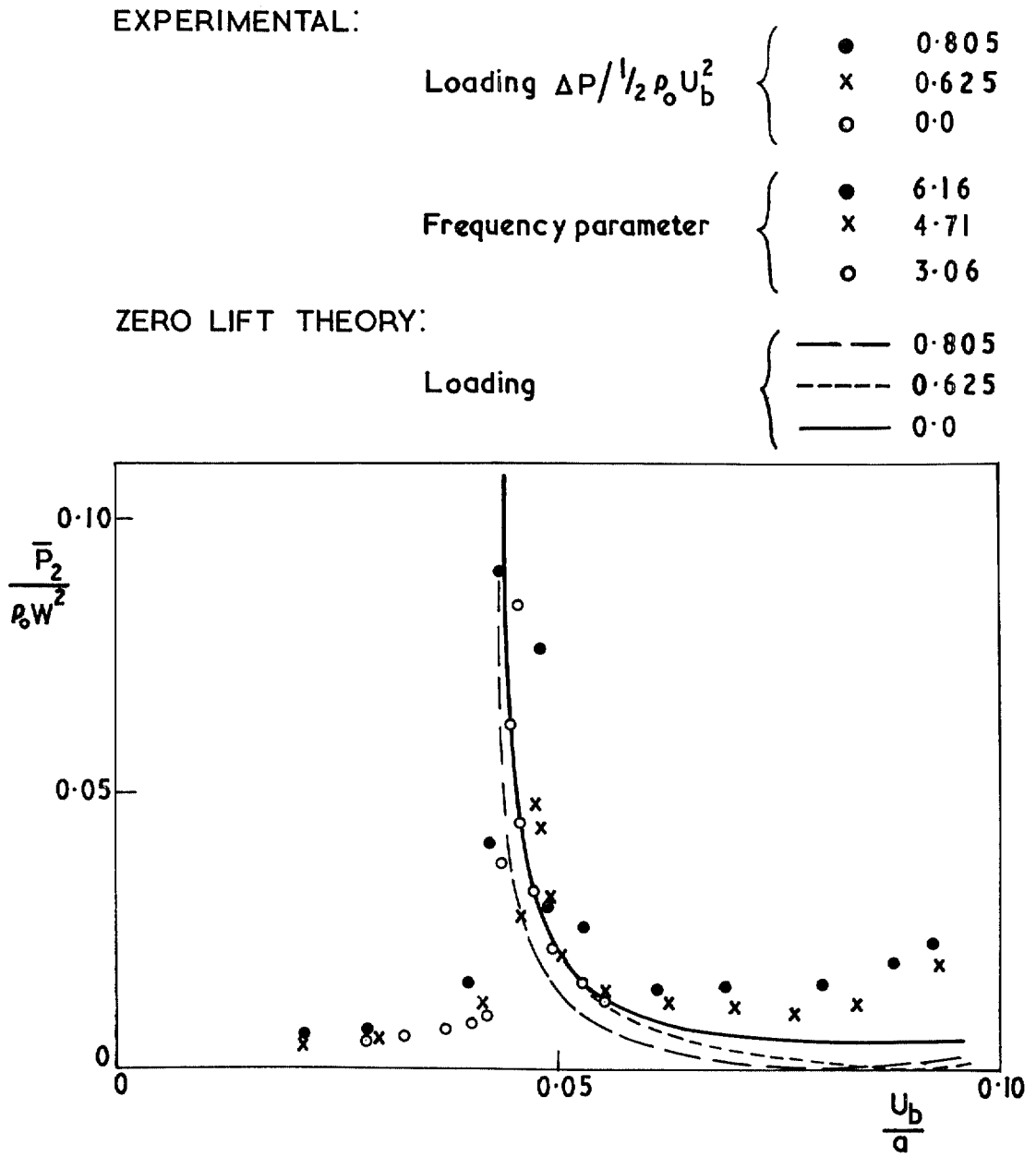

FIG. 20. Downstream acoustic waves.

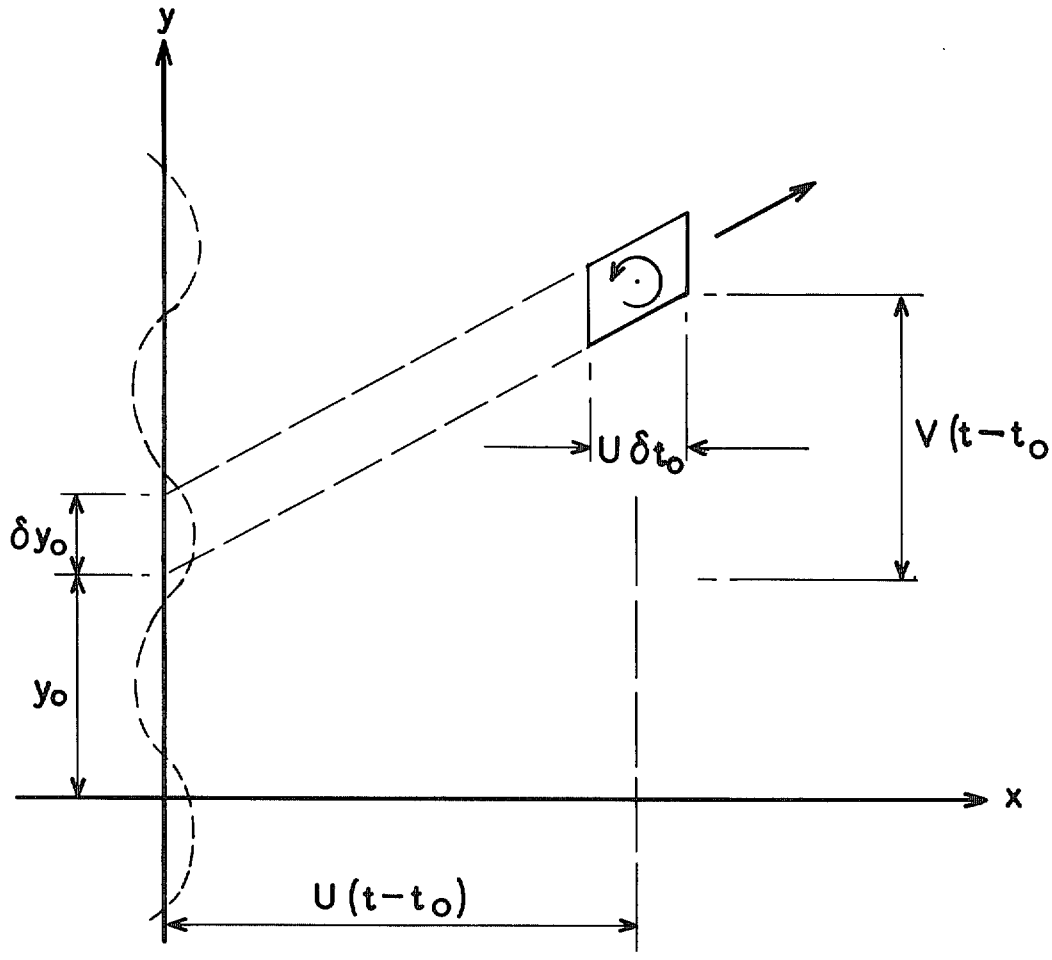

FIG. 21. Diagram showing the situation discussed in Appendix II.

Printed in England for Her Majesty's Stationery Office by J. W. Arrowsmith Ltd., Bristol
Dd. 503426 K.5. 11/72

HER MAJESTY'S STATIONERY OFFICE
Government Bookshops
49 High Holborn, London WC1V 6HB
13a Castle Street, Edinburgh EH2 3AR
109 St Mary Street, Cardiff CF1 1JW
Brazennose Street, Manchester M60 8AS
50 Fairfax Street, Bristol BS1 3DE
258 Broad Street, Birmingham B1 2HE
80 Chichester Street, Belfast BT1 4JY
Government publications are also available through booksellers

SBN 11 470509 7